COMPUTATION OF BIFURCATION MARGINS BASED ON ROBUST CONTROL CONCEPTS

ANDREA IANNELLI*, MARK LOWENBERG †, AND ANDRÉS MARCOS†

Abstract. This article proposes a framework which allows the study of stability robustness of equilibria of a nonlinear system in the face of parametric uncertainties from the point of view of bifurcation theory. In this context, a branch of equilibria is stable if bifurcations (i.e. qualitative changes of the steady-state solutions) do not occur as one or more bifurcation parameters are varied. The work focuses specifically on Hopf bifurcations, where a stable branch of equilibria meets a branch of periodic solutions. It is of practical interest to evaluate how the presence of uncertain parameters in the system alters the result of analyses performed with respect to a nominal vector field. Note that in this article bifurcation parameters have a different meaning than uncertain parameters. To answer the question, the concept of robust bifurcation margins is proposed based on the idea of describing the uncertain system in a Linear Fractional Transformation fashion. The robust bifurcation margins can be interpreted as nonlinear analogs of the structural singular value, or μ, which provides robust stability margins for linear time invariant systems. Their computation is formulated as a nonlinear program aided by a continuation-based multi-start strategy to mitigate the issue of local minima. Application of the framework is demonstrated on two case studies from the power system and aerospace literature.

Key words. Bifurcations, numerical continuation, robust control theory, robust stability

AMS subject classifications. 34C23, 34H20, 37G15, 93D09

1. Introduction.

Bifurcation analysis studies qualitative changes in the response of a nonlinear system (e.g. number and type of steady-state solutions) when one or more parameters on which the dynamics depend are continuously varied [27, 21]. This is usually accomplished by selecting a few *bifurcation parameters*, typically equal in number to the codimension of the studied bifurcation, based on their importance for the system. This analysis approach is of recognized importance since it allows complex dynamic behaviours to be characterized and an understanding of the system to be gained. However, it does not provide indications on the robustness of the results to uncertainties in the models. Let us consider for example the presence of *uncertain parameters* allowed to vary within a prescribed range. These parameters reflect the fact that uncertainty is ubiquitous in engineering systems and at any stage of analysis (from preliminary to detailed). Unlike the bifurcation parameters, in principle they are not restricted in number (and are allowed to vary simultaneously) and their influence on the dynamics may not be known a priori. It is then important to estimate their effect, and in particular whether bifurcation points can move closer to operating points deemed safe on the basis of analyses applied to the nominal system.

The study of robustness within a dynamical systems perspective can be attempted by adopting singularity theory techniques (e.g. Lyapunov-Schmidt reduction) [18], as shown by recently published research [20, 8]. The central idea is to perform a reduction of the original dynamics to a lower dimension map, whose singularities represent transitions between qualitatively different bifurcation diagrams. Even though it is in principle possible to track these singularities without computing explicitly the reduction [8], the application of these techniques to systems with a moderately complex mathematical description and with generic number of uncertainties is not straight-

*Department of Information Technology and Electrical Engineering, Swiss Federal Institute of Technology (ETH), Zürich 8092, Switzerland (iannelli@control.ee.ethz.ch).

†Department of Aerospace Engineering, University of Bristol, BS8 1TR, United Kingdom (m.lowenberg/andres.marcos@bristol.ac.uk).

forward and has not been presented in the literature yet. Moreover, this approach does not directly provide information on the *distance* from a given (nominally stable) operating point to the closest bifurcation, that is, a margin to the bifurcation. Another approach which considers the effect of uncertainties by focussing on a reduced dimensional dynamics, namely the one on the centre manifold, is that proposed in [38]. The main difficulty resides here in the definition of appropriate initial conditions allowing a projection of the long term dynamics on the centre manifold which accurately incorporates the effect of uncertainties [37].

This article proposes a framework which provides a quantitative measure of the distance between branches of stable equilibria and of periodic oscillations in the uncertainty space. In other words, the onset of a Hopf bifurcation in the face of worst-case combinations of the uncertainty is formalised by means of a robust bifurcation margin. Previous works in the literature looked at the problem of computing perturbations to bifurcations. For example, in [12] an extension to multidimensional parameter spaces of standard methods for codimension-1 bifurcations is proposed. The problem of determining locally closest bifurcations is solved by introducing a normal vector to hypersurfaces of bifurcation points, and makes use of both direct and iterative methods. While the latter is limited to static bifurcations (i.e., saddle node, transcritical, and pitchfork), the former is in principle applicable also to the Hopf case. The direct method consists of solving the full set of equations defining the bifurcation (plus additional equations to close the problem) and, as pointed out by the authors of [12], it may be too onerous from a computational point of view. This approach was applied in [32] to the analysis of static bifurcations in flexible satellites, making a number of simplifying assumptions, e.g., no dependence of the equilibrium on the uncertainties and the system having Hamiltonian dynamics. A closely related approach, which according to their authors generalizes the method from [12], is discussed in [6]. The work considers saddle-node bifurcations only, and the computation of the smallest perturbation to bifurcation is done by applying the generalized reduced-gradient method. In essence, this consists of a nonlinear optimization strategy making use of corrector and predictor steps and solving the system of equations defining the bifurcation. However, the issue of local minima is not addressed and the same objection regarding the total dimension of the problem is envisaged for the Hopf bifurcation case (not discussed in that work). The idea of using vectors normal to a manifold of bifurcation points is also present in [16, 34] and other works from the same group, where the design of robustly stable and feasible processes is pursued.

The problem is studied in this article from the point of view of Linear Fractional Transformation (LFT) models and structured singular value (μ) analysis from robust control theory [48]. These tools are well established for the analysis of linear uncertain systems, and provide an analytical answer to stability and performance problems. Even though a direct application to the nonlinear context is precluded by their inherently linear formulation, an extension is proposed here for computing robust bifurcation margins. The core idea is to build an LFT model of the Jacobian of the uncertain vector field (which will generically depend on the states of the system and on the uncertainties) and to formulate the computation of the closest Hopf bifurcation as the worst-case perturbation matrix for which the LFT becomes singular. This bears similarities to the problem solved by μ, but significant differences hold as commented in the paper. The determination of the margins is posed as a nonlinear smooth optimization problem, which can be solved with off-the-shelf algorithms. The program also allows the type of Hopf bifurcation (subcritical or supercritical) to be specified by constraining the sign of the first Lyapunov coefficient. Since the optimization problem is nonlinear, the issue of local minima is discussed and different strategies are proposed to mitigate it. These include a multi-start strategy based on the construction of a manifold of Hopf points connected to a given solution obtained by the optimizer. The main advantages of the proposed approach, whose formulation is detailed in section 3, include: low dimension and computational cost of the solved problem; improved confidence on the accuracy of the results in terms of global validity of the optimum; possibility to apply the wealth of analysis strategies available with μ (e.g., sensitivity analysis, frequency interpretation of the results).

In section 4 the use of this framework to study nonlinear stability problems arising in power system and aerospace applications is investigated by considering two case studies from the literature. First, the sensitivity to a set of physical parameters of the Hopf bifurcation encountered in a power load system with voltage regulator and dynamic load model is considered in section 4.1. It is shown that the application of the robust bifurcation margin allows on one hand to retrieve the same findings reported in [13] (which considered a first-order approximation of the sensitivity), and on the other to investigate more sophisticated types of sensitivity analyses where coupling among uncertain parameters are also accounted for.

Then, an aeroelastic flutter case study is analyzed in section 4.2. Flutter is a self-excited instability in which aerodynamic forces on a flexible body couple with its natural vibration modes producing oscillatory motion. In the presence of nonlinearities, the system typically exhibits loss of stability of the equilibrium in the form of a Hopf bifurcation with ensuing Limit Cycle Oscillations (LCO). Results show a good match with prior studies that considered linear robust analyses [25], and highlight the unique capability of this framework to allow the type of Hopf bifurcation (subcritical or supercritical) of which robustness is studied to be chosen in the analysis.

Bifurcation analysis has been extensively applied to both application fields [41, 11], but the effect of uncertainties has received far less attention. The results in section 4 show that the proposed framework can be a valuable tool for analyzing robustness in the nonlinear context and a more in depth application to these challenging problems is a future research direction.

Preliminary results of this work were presented in [24].

Notation: $[x; y]$ denotes vertical concatenation of two vectors $x \in \mathbb{R}^n$ and $y \in \mathbb{R}^m$. $|\mathbb{I}|$ indicates cardinality of a set $\mathbb{I}$, $\bar{\sigma}(P)$ is the maximum singular value of a matrix $P \in \mathbb{R}^{n\times n}$, $\bar{r}$ is the complex conjugate of $r \in \mathbb{C}^n$ and $\langle r, q\rangle = \bar{r}^T q$ is the scalar product between complex vectors $r, q \in \mathbb{C}^n$. Where evident from the context, subscripts of vectors and matrices are used to specify their elements (e.g., x_3 is the third element of $x \in \mathbb{R}^n$); the symbol $\hat{}$ is used for solutions of an optimization; the symbol $\tilde{}$ is used for uncertain quantities; $\mathrm{diag}(\cdot)$ indicates a block diagonal matrix made up of elements in $\cdot$.

2. Background.

This section provides an overview on the techniques and tools employed in the work. The first subsection presents the theoretical background of bifurcation (2.1.1) and numerical continuation (2.1.2). This is followed by a short introduction to the robust control concepts of LFT models (2.2.1) and μ analysis (2.2.2).

2.1. Nonlinear dynamics approaches.

2.1.1. Bifurcation theory.

Consider an autonomous nonlinear system of the form

$$\dot{x} = f(x, p), \tag{2.1}$$

where $x \in \mathbb{R}^{n_x}$ and $p \in \mathbb{R}^{n_p}$ are respectively the vectors of states and bifurcation parameters, and $f : \mathbb{R}^{n_x} \times \mathbb{R}^{n_p} \to \mathbb{R}^{n_x}$ is the vector field. In this work f is assumed to gather smooth nonlinear functions ($f \in \mathcal{C}^\infty$). Therefore, the Jacobian matrix of the vector field $\nabla_x f : \mathbb{R}^{n_x} \times \mathbb{R}^{n_p} \to \mathbb{R}^{n_x \times n_x}$, denoted here by J, is always defined.

The vector x_0 is called a fixed point or equilibrium of (2.1) corresponding to p_0 if $f(x_0, p_0) = 0$. Let us denote with n_0 the number of eigenvalues of $J(x_0, p_0)$ with zero real parts, respectively. Then x_0 is called a hyperbolic fixed point if $n_0 = 0$, otherwise it is called nonhyperbolic. Bifurcations of fixed points are concerned with the loss of hyperbolicity of the equilibrium as p is varied. Two scenarios can take place: static bifurcations and dynamic bifurcations [27, 21]. The former arise when J is singular at an equilibrium, i.e., it has a zero eigenvalue. The common feature of static bifurcations is that branches of fixed points meet at the bifurcation point. In the case of dynamic bifurcations, branches of fixed points and periodic solutions meet. This case, also referred to as Hopf bifurcation, is the focus of this work and is formally described by the following theorem.

THEOREM 2.1 ([21] Hopf bifurcation theorem). *Suppose that the system $\dot{x} = f(x, p)$, $x \in \mathbb{R}^{n_x}$ and $p \in \mathbb{R}$ has an equilibrium (x_H, p_H) at which the following properties are satisfied.*

1. *$J(x_H, p_H)$ has a simple pair of pure imaginary eigenvalues and no other eigenvalues with zero real parts. This implies, for the implicit function theorem, that there is a smooth curve of equilibria $(x(p), p)$ with $x(p_H) = x_H$. The eigenvalues $\nu(p)$, $\bar{\nu}(p)$ of $J(x(p))$, with $\nu(p_H){=}i\omega_H$, vary smoothly with p.*
2. *It holds*

$$\frac{d}{dp} \left(\operatorname{Re} \nu(p)\right)\big|_{p=p_H} = l_0 \neq 0. \tag{2.2}$$

Then there is a unique three-dimensional center manifold passing through (x_H, p_H) in $\mathbb{R}^{n_x} \times \mathbb{R}$ and a smooth system of coordinates for which the Taylor expansion of degree 3 on the center manifold is given in polar coordinates (ρ, θ) by

$$\begin{aligned} \dot{\rho} &= (l_0 p + l_1 \rho^2)\rho, \\ \dot{\theta} &= \omega + l_2 p + l_3 \rho^2, \end{aligned} \tag{2.3}$$

where l_0, l_1, l_2, and l_3 are real coefficients defining the manifold. If $l_1 \neq 0$, there is a surface of periodic solutions in the center manifold which has quadratic tangency with the eigenspace of $\nu(p)$, $\bar{\nu}(p)$. If $l_1 < 0$, then these periodic solutions are stable limit cycles, while if $l_1 > 0$, the periodic solutions are repelling.

Note first that the theorem is typically stated considering a scalar p since the Hopf bifurcation is codimension-1. Condition 1 of Th. 2.1 requires that the Jacobian of the vector field has a pair of purely imaginary eigenvalues (and no other eigenvalues on the imaginary axis). Condition 2, also known as the transversality condition, prescribes that these eigenvalues are not stationary with respect to p at the bifurcation. A fundamental parameter determining the dynamic behaviour in the neighborhood of a Hopf point is l_1, also called the first Lyapunov coefficient. Its value determines whether the Hopf bifurcation is *subcritical* or *supercritical*, and its analytical expression is given by [27]

$$l_1 = \frac{1}{2\omega_H} \operatorname{Re}\langle r, C(q, q, \bar{q}) - 2B(q, A^{-1}B(q, \bar{q})) + B(\bar{q}, (2i\omega_H I_n - A)^{-1} B(q, q))\rangle. \tag{2.4}$$

Here the complex vectors r, $q \in \mathbb{C}^{n_x}$ satisfy

$$Jq = i\omega_H q, \qquad J^T r = -i\omega_H r, \qquad \langle r, q\rangle = 1. \tag{2.5}$$

The functions $B : \mathbb{R}^{n_x} \times \mathbb{R}^{n_x} \to \mathbb{R}^{n_x}$ and $C : \mathbb{R}^{n_x} \times \mathbb{R}^{n_x} \times \mathbb{R}^{n_x} \to \mathbb{R}^{n_x}$ are the tensors of second and third order derivatives evaluated at x_H, respectively. For example, for vectors ξ, ς, $\chi \in \mathbb{R}^{n_x}$, $B(\xi, \varsigma)$ and $C(\xi, \varsigma, \chi)$ are in $\mathbb{R}^{n_x}$ with components

$$\begin{aligned} B_i(\xi,\varsigma) &= \sum_{j,k=1}^{n_x} \frac{\partial^2 f_i(x,p)}{\partial x_j x_k}\bigg|_{x=x_H, p=p_H} \xi_j \varsigma_k, \quad i = 1, 2, ..., n_x, \\ C_i(\xi,\varsigma,\chi) &= \sum_{j,k,l=1}^{n_x} \frac{\partial^3 f_i(x,p)}{\partial x_j x_k x_l}\bigg|_{x=x_H, p=p_H} \xi_j \varsigma_k \chi_l, \quad i = 1, 2, ..., n_x. \end{aligned} \tag{2.6}$$

2.1.2. Numerical continuation. The computational tool of bifurcation analysis is numerical continuation, providing path following algorithms allowing implicitly defined manifolds [19] to be computed. These schemes are based on the implicit function theorem (IFT) [45], which guarantees, under the condition that J is non-singular at an initial point (x_0, p_0), that there exist neighbourhoods X of x_0 and P of p_0 and a function $g : P \to X$ such that $f(x, p) = 0$ has the unique solution $x = g(p)$ in X. Examples of numerical techniques to compute the implicit manifold g are Newton-Raphson, arclength, and pseudo-arclength continuation [19], efficiently implemented in freely available software, e.g., AUTO [14], and COCO [10].

A general continuation problem, so called *extended*, can be formulated as follows [9, 10]

$$\begin{aligned} &F(u,\lambda) := \begin{pmatrix} \Phi(u) \\ \Psi(u) \end{pmatrix} - \begin{pmatrix} 0 \\ \lambda \end{pmatrix} = 0, \\ &\Phi : \mathbb{R}^{n_u} \to \mathbb{R}^m, \qquad \Psi : \mathbb{R}^{n_u} \to \mathbb{R}^{n_\lambda}, \end{aligned} \tag{2.7}$$

where Φ defines the zero problem in the vector u of continuation *variables*, Ψ denotes a family of monitor functions and λ is a vector of continuation *parameters*. It is straightforward to see that the goal of tracking equilibria of the vector field f can be pursued by solving the zero problem only with $\Phi = f$, and $u = [x; p]$. However, the extended continuation problem in (2.7) allows for a greater variety of problems to be solved, as the related concept of *restricted* continuation problem shows. Let $\mathbb{I} \subseteq \{1, ..., n_\lambda\}$ be an index set and $\bar{\mathbb{I}}$ its complement in $\{1, ..., n_\lambda\}$. Let $\lambda_{\mathbb{I}} = \{\lambda_i | i \in \mathbb{I}\}$ and consider the restriction $F(u, \lambda)|_{\lambda_{\mathbb{I}} = \lambda^*_{\mathbb{I}}}$ satisfying the IFT at some point $(u^*, \lambda^* = \Psi(u^*))$. Then $F(u, \lambda)|_{\lambda_{\mathbb{I}} = \lambda^*_{\mathbb{I}}}$ defines a continuation problem for a d-manifold with $d = n_u - (m + |\mathbb{I}|)$. $\lambda_{\bar{\mathbb{I}}}$ and $\lambda_{\mathbb{I}}$ are called the set of active and inactive continuation parameters respectively, since the former changes during continuation, while the latter remain constant. Analogously, equations corresponding to $\lambda_{\bar{\mathbb{I}}}$ are inactive constraints, while equations corresponding to $\lambda_{\mathbb{I}}$ are active constraints, because they impose an additional condition on the solutions to the set of zero problems. The formulation (2.7) is implemented in the software COCO, which is used for all the continuation analyses performed in this work.

2.2. Robust control theory.

2.2.1. The Linear Fractional Transformation paradigm. Linear Fractional Transformation (LFT) is an instrumental tool in robust control theory for analysis and control of uncertain systems [48]. For the sake of clarity, first an intuition of the reasoning behind LFT is given, followed by a more formal definition.

The classic interpretation of an LFT is in terms of input to output relationship of a feedback interconnection. Let us consider a linear time invariant (LTI) system with transfer matrix (i.e. matrix of transfer functions) $M_{22} \in \mathbb{C}^{p_2 \times q_2}$, input v and output y. The system M_{22} is assumed to be exactly known, and thus is also termed *nominal*. If the model has uncertainties (which will be better characterized later), these can be modelled with an operator $\Delta_u \in \mathbb{C}^{q_1 \times p_1}$ with input z and output w. The effect of Δ_u on M_{22} can then be described by introducing the transfer matrices M_{11}, M_{12} and M_{21}. For example, in the case of parametric uncertainties, these will be simply static (gain) matrices, while for the case of unmodelled dynamics these could also have dynamic terms (e.g. low pass filters). The key point is that, by choosing these matrices, the analyst can describe with a certain flexibility how the perturbation affects the nominal system. Given this setting, Figure 1 shows the standard representation of LFT.

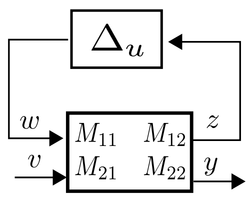

$$
\begin{aligned}
w &= \Delta_u z \\
z &= M_{11} w + M_{12} v \\
y &= M_{21} w + M_{22} v
\end{aligned}
$$

Fig. 1. *Standard feedback representation of an LFT.*

The central idea is thus to represent the uncertain system as a feedback of known components (the transfer matrices M_{ij}) with uncertain (the operator Δ_u) ones. In practice, this is done by pulling out of the system the unknown parts, so that the problem appears as a nominal system subject to an artificial feedback. Available toolboxes [28] allow this operation to be efficiently performed and provide the analyst, given a description of how the uncertainties affect the system, with the matrices M_{ij}.

In order to formally define an LFT, let us denote by $M \in \mathbb{C}^{(p_1+p_2)\times(q_1+q_2)}$ the partitioned transfer matrix (also termed *coefficient matrix*)

$$
M = \begin{bmatrix} M_{11} & M_{12} \\ M_{21} & M_{22} \end{bmatrix}, \tag{2.8}
$$

and let $\Delta_u \in \mathbb{C}^{q_1 \times p_1}$ the uncertain operator. The LFT of M with respect to Δ_u is defined as the map $\mathcal{F} : \mathbb{C}^{q_1 \times p_1} \longrightarrow \mathbb{C}^{p_2 \times q_2}$

$$
\mathcal{F}(M, \Delta_u) = M_{22} + M_{21}\Delta_u (I - M_{11}\Delta_u)^{-1} M_{12}. \tag{2.9}
$$

With reference to Fig. 1, $\mathcal{F}(M, \Delta_u)$ compactly defines the uncertain transfer matrix from input v to output y of the nominal system M_{22} when this is subject to Δ_u. Indeed, for $\Delta_u = 0$ (no uncertainties in the model) it holds $\mathcal{F}(M, \Delta_u) = M_{22}$. It is also important to observe that M_{11} is, within this input to output framework, the transfer matrix seen by the perturbation block Δ_u. A crucial feature apparent in (2.9) is that the LFT is well posed if and only if the inverse of $(I - M_{11}\Delta_u)$ exists. Otherwise, $\mathcal{F}(M, \Delta_u)$ is said to be singular. Singularity of the LFT is typically associated with the loss of stability of the underlying uncertain system, and thus finding the uncertain perturbations for which this happens is typically the objective of robust stability analysis (details on this will be provided in Sec. 2.2.2).

In robust control, Δ_u typically gathers parametric and dynamic uncertainties and can be represented as

$$\Delta_u = \mathrm{diag}(\delta_i I_{d_i}, \delta_j I_{d_j}, \Delta_{D_k}),$$
$$i = 1, ..., n_R, \quad j = n_R + 1, ..., n_R + n_C, \quad k = 1, ..., n_D, \tag{2.10}$$

where the uncertainties associated with n_R real scalars δ_i, n_C complex scalars δ_j, and n_D unstructured (or full) complex blocks Δ_{D_k} are listed in diagonal format. The identity matrices of dimension d_i and d_j take into account the fact that scalar uncertainties might be repeated in Δ_u when the LFT of the system is built up. For example, if a matrix has the parameter δ_i on three different rows, in order to cast it in the form of an LFT (2.9) it will be necessary to have d_i=3 [28]. Typically the uncertain parameters are normalized by scaling of M such that $\Delta_u = 0$ coincides with the nominal system (i.e., uncertain parameters at their nominal values) and $\bar{\sigma}(\Delta_u) \leq 1$ when uncertainties take values in the allowed interval. The set in (2.10) is generally referred to as *structured* because of the block diagonal structure. This feature, enabled by the LFT modeling paradigm, is known to provide less conservative results in the analysis of uncertain systems with respect to unstructured representations (used, for example, in the celebrated small gain theorem [48]).

This work leverages the LFT framework for analysis of nonlinear systems. The interpretation given previously, while providing insights into this paradigm, cannot be thus readily used since it requires transfer matrices. For this reason, an alternative viewpoint on LFT is proposed.

Let us start by considering the state-space (SS) representation $(\mathcal{A}, \mathcal{B}, \mathcal{C}, \mathcal{D})$ of the nominal LTI system with transfer matrix M_{22}

$$\begin{cases} \dot{x} = \mathcal{A}x + \mathcal{B}v, \\ y = \mathcal{C}x + \mathcal{D}v, \end{cases} \tag{2.11a}$$

$$M_{22}(s) = \mathcal{D} + \mathcal{C}(sI_{n_x} - \mathcal{A})^{-1}\mathcal{B}, \tag{2.11b}$$

where s is the Laplace variable. Define now

$$M_\nu = \begin{bmatrix} \mathcal{A} & \mathcal{B} \\ \mathcal{C} & \mathcal{D} \end{bmatrix}, \qquad \Delta_\nu = \frac{1}{s} I_{n_x}. \tag{2.12}$$

It can then be shown that $\mathcal{F}(M_\nu, \Delta_\nu) = M_{22}$. This follows directly from

$$\mathcal{F}(M_\nu, \Delta_\nu) = \mathcal{D} + \mathcal{C}\frac{1}{s}I_{n_x}(I_{n_x} - \frac{1}{s}\mathcal{A})^{-1}\mathcal{B} = \mathcal{D} + \mathcal{C}(sI_{n_x} - \mathcal{A})^{-1}\mathcal{B} = M_{22}(s), \tag{2.13}$$

where the diagonal structure of Δ_ν and the fact that $\frac{1}{s} \neq 0$ have been exploited. This result shows that the LFTs generalize the realization of transfer matrices into state-space (SS) representations to the case of rational multivariate matrices. For this reason, the LFT paradigm can also be regarded as a realization technique [28].

This interpretation also highlights a paramount aspect for the present work. The poles of (2.11) are typically found via eigenvalue analysis of $\mathcal{A}$. Equivalently, the system has a given pole ν if $(\nu I_{n_x} - \mathcal{A})^{-1}$ is singular. Note that this latter condition can be formulated as the singularity of the LFT $\mathcal{F}(M_\nu, \Delta_\nu)$ by replacing $s = \nu$. In particular, the LTI (2.11) has a purely imaginary eigenvalue (i.e. it is neutrally stable) if there exists $\omega > 0$ for which $\mathcal{F}(M_\nu, \Delta_\nu)$ is singular with $s = i\omega$.

Let us consider now the case when the LTI system (2.11) is subject to uncertainties. The problem can be described with the LFT formalism considering two blocks for the *uncertain* operator, namely Δ_u containing the structured perturbations, and Δ_ν. The coefficient matrix M is partitioned correspondingly

$$M = \begin{bmatrix} \mathcal{A} & \mathcal{A}_{12} & \mathcal{B} \\ \mathcal{A}_{21} & \mathcal{A}_{22} & \mathcal{B}_1 \\ \mathcal{C} & \mathcal{C}_1 & \mathcal{D} \end{bmatrix}, \qquad \Delta = \mathrm{diag}(\Delta_\nu, \Delta_u). \tag{2.14}$$

A pictorial representation of the LFT $\mathcal{F}(M, \Delta)$ defined by the operators in (2.14) is given in Figure 2.

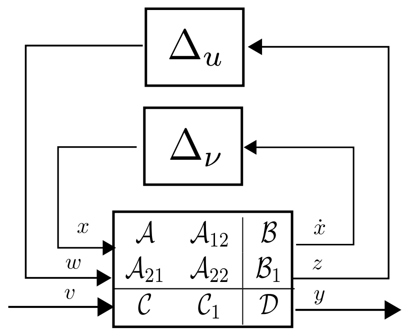

Fig. 2. *LFT of an uncertain state-space model.*

The difference between the representations in Figure 1 and Figure 2, both describing an uncertain system, is that in the former the system is described via its transfer matrices, while in the latter a state-space representation is used. One can switch from the first to the second representation by exploiting the fact that $\mathcal{F}(M_\nu, \Delta_\nu) = M_{22}$ (which was proved above).

The consequence of this change of representation is that the new block Δ_ν appears. Correspondingly, the coefficient matrix M (2.14) now features the matrix M_ν (2.12) plus other matrices describing the effect of the uncertainties on the state-matrices. Note indeed that the transfer matrices M_{11}, M_{12} and M_{21} will also be expressed here with their SS representation. Let us assume now that (2.11) is nominally stable (i.e. $\mathcal{A}$ has all the eigenvalues in the left half-plane). Then the uncertain LTI system has a purely imaginary eigenvalue if there exist $\omega > 0$ (with $s = i\omega$) and a combination of the uncertainties in Δ_u for which $\mathcal{F}(M, \Delta)$ (2.14) is singular.

The advantage of this representation, which is key for the present work, is that LFTs can be constructed even for systems which do not have transfer matrices, if an *appropriate* state-space description is available. Sec. 3.1 will be devoted to showing which crucial steps can be taken in order to apply this rationale to the prototype of vector field introduced in (2.1).

Note finally that a useful property when dealing with LFTs featured by distinct Δ-blocks is that interconnections of LFTs can be rewritten as one single LFT. This is only a numerical aspect relative to the construction of LFT models, but it greatly helps to separate modeling-specific details of the system under consideration and to ease the algebraic manipulations. By virtue of this, it holds for the LFT defined in (2.14)

$$\mathcal{F}(M, \Delta) = \mathcal{F}(\mathcal{F}(M, \Delta_\nu), \Delta_u). \tag{2.15}$$

2.2.2. μ analysis. The μ analysis technique leverages the key features of LFT modeling reviewed in the previous section to address the robust stability analysis of

LTI systems in the face of uncertainties. The structured singular value is a matrix function denoted by $\mu_\Delta(M)$ and several equivalent definitions are available in the literature [48, 15, 35]. A definition which encompasses the aspects relevant to this work is

$$\mu_\Delta(M) = \left(\min_{\Delta} (\kappa :\ \mathcal{F}(\mathcal{F}(M, \Delta_\nu), \Delta_u) \text{ is singular},\ \ \bar{\sigma}(\Delta_u) \leq \kappa \right)^{-1}, \tag{2.16}$$

where κ is a real positive scalar, and $\mu_\Delta(M) = 0$ if the minimization problem has no solution.

Based on the point of view of LFT as realization technique, an interpretation of the μ analysis technique is as *worst-case* eigenvalue analysis for uncertain systems. Let us focus on the operator Δ of the LFT $\mathcal{F}(M, \Delta)$ defined in (2.14). The block Δ_ν does not represent a true uncertainty of the system, and its meaning is that the singularity of the LFT is checked against all the possible eigenvalues on the imaginary axis. For the sake of understanding, one can think of realizing this block by considering a set of frequencies ω and evaluating Δ_ν at $\nu = i\omega$. By doing this, $\Delta = \Delta_u$ and the problem defined in (2.16) consists of finding the perturbation matrix with the smallest maximum singular value (also termed worst-case matrix) such that the uncertain system has a pair of purely imaginary eigenvalues $\pm i\omega$. Therefore, $\mu_\Delta(M)$ provides a robust stability (RS) test for an uncertain linear system. Specifically, if $\mu_\Delta(M) \geq 1$ a candidate (i.e., within the allowed range of the uncertainty set) perturbation matrix exists that violates the well-posedness of $\mathcal{F}(M, \Delta)$. In essence, the uncertain state-matrix has the eigenvalues $s = \pm i\omega$ for a certain combination of the uncertainties in the allowed range. On the contrary, if $\mu_\Delta(M) < 1$ then there is no perturbation matrix inside the set Δ such that the $\mathcal{F}(M, \Delta)$ is ill-posed and thus the system is robust stable within the range of uncertainties considered.

In the most established algorithms [2], μ is evaluated on a discretized frequency range. That is, the Δ_ν block is realized as discussed before on a pre-selected grid of frequencies, and the corresponding set of matrices $M(i\omega)$ (the dependence on the frequency is now stressed) is computed. Subsequently, $\mu_\Delta(M(i\omega))$ is computed and a frequency-domain representation of the results is obtained. This is done in order to avoid the need to solve the optimization problem (2.16) on a continuous range of frequency, which proves computationally challenging. An exception to this common practice worth mentioning is represented by recently developed Hamiltonian-based algorithms (i.e. SMART library [39] and Robust Control Toolbox from MATLAB R2016b) which guarantees the validity of results over a continuous range of frequencies.

Finally, note that (2.16) is an NP-hard problem with either pure real or mixed real-complex uncertainties [5], thus all μ algorithms work by searching for upper and lower bounds. The upper bound μ_{UB} provides the maximum size perturbation $\bar{\sigma}(\Delta_u^{UB}) = 1/\mu_{UB}$ for which RS is guaranteed, whereas the lower bound μ_{LB} defines a minimum size perturbation $\bar{\sigma}(\Delta_u^{LB}) = 1/\mu_{LB}$ for which RS is guaranteed to be violated. Along with this information, the lower bound also provides the matrix Δ_u^{LB} determining singularity of the LFT.

3. Main results. In this section the main result of the work is presented. The problem addressed by this article is formally defined in section 3.1 and in section 3.2 a solution by means of a nonlinear optimization program is proposed. The step-by-step presentation, from Program 3.1, which calculates the *smallest* perturbations making the Jacobian unstable, to Program 3.4, which computes the closest subcritical and supercritical Hopf bifurcations, aims at clearly presenting the formulation of robust bifurcation margins. Note that only Program 3.2 and Program 3.4 are actually needed to solve the problem (depending on whether the type of Hopf bifurcation is specified or not). In section 3.3 a multi-start strategy is described, within the extended continuation paradigm, to mitigate the issue of local optima. Finally, in section 3.4 a critical comparison with an alternative method from the literature solving a similar problem is discussed.

3.1. Problem statement. The usual starting point in bifurcation analysis is Eq. (2.1), where f is a *nominal* vector field, meaning that the only dependence is on the state x and bifurcation parameter p. The latter is of size $n_p = 1$ for continuation of equilibrium points since all their bifurcations have codimension 1, and thus 1 parameter is sufficient for its analysis (this of course includes the case of Hopf bifurcations, see Theorem 2.1). Consider the case when parametric uncertainties affect the dynamics, e.g. because of lack of confidence on the values of model parameters or simplifying assumptions underlying the model. The presence of uncertainties can be modelled by introducing the uncertainty vector δ

$$\delta = [\delta_1; ...; \delta_i; ...\delta_{n_\delta}], \quad \delta \in \mathbb{R}^{n_\delta}. \tag{3.1}$$

The vector field depends now on δ, in addition to x and p. To highlight this, we denote the uncertain vector field by $\tilde{f}$ and the associated Jacobian by $\tilde{J}$

$$\dot{x} = \tilde{f}(x, p, \delta), \tag{3.2a}$$

$$\tilde{f} : \mathbb{R}^{n_x} \times \mathbb{R} \times \mathbb{R}^{n_\delta} \to \mathbb{R}^{n_x}, \quad \tilde{f} \in \mathcal{C}^\infty, \tag{3.2b}$$

$$\tilde{J} : \mathbb{R}^{n_x} \times \mathbb{R} \times \mathbb{R}^{n_\delta} \to \mathbb{R}^{n_x \times n_x}. \tag{3.2c}$$

The objective of the work is then to compute the margins of stable equilibria from the closest Hopf bifurcation for nonlinear systems affected by parametric uncertainties. To better understand this, assume that the nominal system f has a Hopf bifurcation point (x_H, p_H), while for another value of the bifurcation parameter $\bar{p}_0$ a stable fixed point $\bar{x}_0$ exists for f. The goal is to determine the *smallest* (or *worst-case*) perturbation $\bar{\delta} \in \delta$ such that $\tilde{f}$ undergoes a Hopf bifurcation at $\bar{p}_0$. It is key to observe that the Hopf bifurcation is triggered by perturbations in δ, while the bifurcation parameter is fixed at $\bar{p}_0$. The reason for this is that the aim here is to compute the *margin* of a certain condition from the occurrence of the bifurcation. Thus, p, which generally defines an operating condition (e.g. load power in an electric power system, speed for an aircraft) is kept fixed at the value $\bar{p}_0$ which identifies the condition for which the margin is computed. This is different from what is done in the direct method [12] (the other approach that looked at a similar problem) where there is no distinction between bifurcation and uncertain parameters, both collected in p (which is then multidimensional). As a result of this, all the entries of p are allowed to be perturbed in order to trigger the bifurcation, whereas here the distinction between p (of dimension 1) and δ (of dimension n_δ, depending on how many uncertainties are considered) is clear. See section 3.4 for a thorough comparison with the direct method.

It is often relevant to distinguish between supercritical and subcritical Hopf bifurcations, hence two distinct worst-case perturbations will be considered. For the sake of readability, this distinction will be highlighted in the text when relevant but the notation used will be $\bar{\delta}$ in both cases.

In order to quantify the margin to the closest bifurcation, and thus to allow the concept of worst-case uncertainty to be formalized, a metric for the magnitude of the perturbation must be adopted. The adopted metric should measure in some quantitative form the perturbation to which the system is subject. This task is arbitrary and a common approach from robust control is followed [48] (see also section 2.2.2).

Consider a generic uncertain parameter d, with w_d indicating the uncertainty level with respect to a nominal value d_0 and $\delta_d \in [-1, 1]$ representing the normalized uncertainty range. Note that d_0 and w_d are typically fixed by the analyst based on the knowledge of the nominal value and dispersion of the parameter d respectively. A multiplicative uncertain representation of d is thus obtained as

$$d = (1 + w_d \delta_d) d_0, \tag{3.3}$$

where $\delta_d = 0$ corresponds to the nominal value of d, while $\delta_d = \pm 1$ represents a perturbation at the extreme of the parameter range (e.g., a variation of $\pm 20\%$ from d_0 if $w_d = 0.2$). Once the normalization (3.3) is applied to all the uncertain parameters in (3.1), a possible scalar metric (or norm) to quantify the magnitude of the perturbation is the largest of the absolute values of the elements in δ. This can be equivalently expressed as $\bar{\sigma}(\text{diag}(\delta))$, i.e., the maximum singular value of the diagonal matrix with elements of δ on the diagonal. Such a metric quantifies the deviation of the uncertain parameters from their nominal values along the direction of the parameter space where this is largest. The objective is thus to compute the perturbation vector with the smallest possible norm, providing therefore the distance from the closest Hopf bifurcation.

In fact, $k_m = \bar{\sigma}(\text{diag}(\delta))$ can be regarded as a robust margin from bifurcation because $k_m \leq 1$ means that a candidate (i.e., within the allowed range of the uncertainty set) perturbation exists which determines a Hopf bifurcation. Thus, the equilibrium $\bar{x}_0$ of the nominal vector field is not robustly stable at $\bar{p}_0$. On the contrary, if $k_m > 1$ then there is no perturbation inside the allowed set which is capable of prompting a Hopf bifurcation. This is pictorially represented in Figure 3, where on the x-axis is reported the bifurcation parameter and on the y-axis the margin k_m (note that the case $\bar{p}_0 < p_H$ where a Hopf bifurcation is encountered by increasing p is assumed here without loss of generality). When the line $k_m = 1$ is crossed, the system is operated in a region where Hopf bifurcations can occur in the face of the uncertainties accounted for in the system (shaded area).

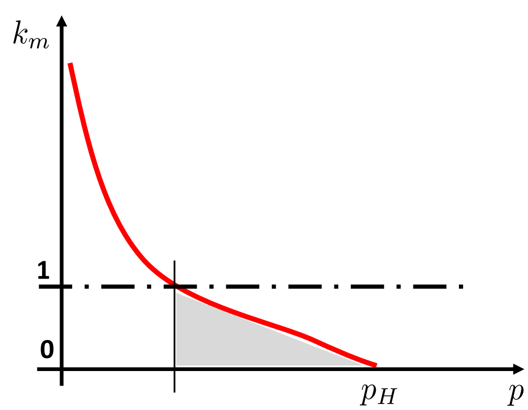

FIG. 3. *Concept of robust bifurcation margins.*

3.2. Solution via nonlinear optimization. The fundamental idea to address the stated objective is to exploit the interpretation of LFTs discussed in Sec. 2.2.1. Consider for a moment only Condition 1 of Theorem 2.1, which prescribes a pair of purely imaginary eigenvalues for the Jacobian. If $\tilde{J}$ is interpreted as the uncertain state-matrix of the linear case, an LFT model of the former with respect to the uncertain parameters in δ can be built up (numerically or analytically [29]). The main difference from the linear case is that in general $\tilde{J}$ is also a function of the states of the system x. This reflects the fact that in the nonlinear context uncertainties have a twofold effect on stability. They directly affect the matrix $\tilde{J}$ as independent variables, but also indirectly by changing the location of the equilibrium (around which the vector field is linearized). The latter is a distinctive feature of the nonlinear setting, since in the linear case the location of the equilibrium does not have any effect on the spectrum of the state-matrix, and thus on stability. In full generality, the LFT of the Jacobian $\mathcal{F}(M_{\tilde{J}}, \Delta)$ can be written as

$$\mathcal{F}(M_{\tilde{J}}, \Delta) = \mathcal{F}(\mathcal{F}(\mathcal{F}(M_{\tilde{J}}, \Delta_\nu), \Delta_x), \Delta_u), \tag{3.4a}$$

$$\Delta = \mathrm{diag}(\Delta_u, \Delta_x, \Delta_\nu), \quad M_{\tilde{J}} = \left[M_{\tilde{J}_{11}} M_{\tilde{J}_{12}}; M_{\tilde{J}_{21}} M_{\tilde{J}_{22}}\right], \tag{3.4b}$$

$$\Delta_u = \mathrm{diag}(\delta_1 I_{d_1}, ..., \delta_i I_{d_i}, ..., \delta_{n_\delta} I_{d_{n_\delta}}), \tag{3.4c}$$

$$\Delta_x = \mathrm{diag}(x_1 I_{x_1}, ..., x_j I_{x_j}, ..., x_{n_x} I_{x_{n_x}}), \tag{3.4d}$$

$$\Delta_\nu = \frac{1}{\nu} I_{n_x}, \quad \nu = i\omega, \tag{3.4e}$$

where (3.4a) exploits the property of interconnected LFTs, and Δ_u is a particular instance of the structured uncertainty set defined in (2.10), considering only real parameters. Compared to the linear case (2.15), Δ features now an additional structured block Δ_x, which arises when performing the LFT modeling of $\tilde{J}$ due to the states explicitly appearing in the Jacobian, and for which a similar representation to the one for Δ_u is employed. Δ_ν finally restricts the attention to purely imaginary eigenvalues of $\tilde{J}$ with frequency ω.

Condition 1 of Theorem 2.1 can then be expressed as the singularity of the LFT (3.4a). This is the central step of the proposed extension of μ from the linear context, where $\tilde{J}$ would be the uncertain state-matrix, to the nonlinear one. In fact, μ computes by definition the worst-case perturbation matrix which makes the underlying LFT ill-posed and employs the same metric (2.16) as the one used to define the robust bifurcation margin k_m. It follows indeed from the definitions and properties commented earlier that $k_m = \bar{\sigma}(\mathrm{diag}(\delta)) = \bar{\sigma}(\Delta_u)$. Specifically, k_m is the reciprocal of μ and it has been adopted here because of its straightforward meaning of distance (or margin) to the onset of a bifurcation. Note in this regard that the symbol k_m was used in the early stages of robust control with the name of *excess stability margin* [43, 42].

The discussion above paves the way for the nonlinear program presented next, which aims to compute the smallest perturbation for which $\tilde{J}$ has a pair of purely imaginary eigenvalues.

PROGRAM 3.1.

$$\min_X k_m \quad \text{such that} \begin{cases} \tilde{f}(x, \bar{p}_0, \delta) = 0, & (3.5a) \\ \mathcal{F}(M_{\tilde{J}}, \Delta) \text{ is singular}, & (3.5b) \\ \bar{\sigma}(\Delta_u) \le k_m, & (3.5c) \end{cases}$$

$$X = [x; \delta; \omega],$$

where X is the vector of optimization variables including: states x; uncertain parameters δ; and frequency ω. $\hat{X}$ will indicate the solution vector gathering $\hat{x}$, $\hat{\delta}$, and $\hat{\omega}$ respectively. Let us examine the constraints of the program. Eq. (3.5a) guarantees that the solution $(\hat{x}, \hat{\delta})$ corresponds to an equilibrium point for the system. Eq. (3.5b) ensures that $\tilde{J}$ has a pair of complex eigenvalues $\nu = \pm\hat{\omega}$, and Eq. (3.5c) bounds the size of the perturbation matrix.

This is a similar optimization problem to that in (2.16), with two crucial differences: constraint (3.5a), and the addition of Δ_x in the block Δ of $\mathcal{F}(M_{\tilde{J}}, \Delta)$ (to which, notably, constraint (3.5c) does not apply). Due to these differences, available algorithms for μ cannot be applied to compute solutions of (3.5), thus alternative ways should be pursued. Let us examine closely (3.5b), which prescribes singularity of an LFT. According to the definition given in (2.9), necessary and sufficient condition for the well-posedness of a generic LFT $\mathcal{F}(M, \Delta_u)$ is the existence of the inverse of the matrix $(I - M_{11}\Delta_u)$. Note that M_{11} is, as also previously observed, the transfer matrix seen by the perturbation block Δ_u. In the context of the LFT $\mathcal{F}(M_{\tilde{J}}, \Delta)$ introduced in (3.4), this means that the singularity constraint (3.5b) holds if and only if $\det(I - M_{\tilde{J}\,11}\Delta) = 0$. This, in turn, can be recast as nonlinear constraints in the optimization variables X.
As for (3.5c), this is a non-smooth constraint because of the maximum singular value operator, but it can be drastically simplified by exploiting the structure of Δ_u (3.4c). Indeed this constraint is equivalent to

$$-k_m \le \delta_i \le k_m, \qquad i = 1, ..., n_\delta, \tag{3.6}$$

which is a set of linear inequalities in the optimization variables and the objective function k_m. Note that a similar relaxation would hold also for complex scalar uncertainties, not considered in this work.

Based on the previous discussion, the following smooth nonlinear optimization problem is proposed to solve Program 3.1.

PROGRAM 3.2.

$$\min_X k_m \quad \text{such that} \begin{cases} \tilde{f}(x, \bar{p}_0, \delta) = 0, & \text{(3.7a)} \\ \det(I - M_{\tilde{J}\,11}\Delta) = 0, & \text{(3.7b)} \\ -k_m \le \delta_i \le k_m, \qquad i = 1, ..., n_\delta, & \text{(3.7c)} \end{cases}$$

$$X = [x; \delta; \omega], \quad n_{ctrs} = n_x + 2 + n_\delta,$$

where n_{ctrs} denotes the number of total constraints of the optimization.

The key idea behind Program 3.2 is to enforce singularity of the LFT (3.5b) by using directly the determinant condition represented by constraint (3.7b). In [40] this is listed among the known methods for the computation of μ_{LB}, and examples of related algorithms can be found in [22, 47]. The approaches presented in those works, however, are limited to the case of linear systems, i.e., they represent alternatives to well-established μ lower bounds algorithms such as the power iteration [36] and the gain-based method [44]. To the best of the authors' knowledge, this is indeed the first time that the concept of structured singular value is used in the context of worst-case bifurcations of a nonlinear vector field. Moreover, Program 3.2 recasts the optimization so that the objective function and the constraints are smooth. This differs from the aforementioned works where the optimization was performed by minimizing the nonsmooth function $\bar{\sigma}(\Delta_u)$. This is overcome here by considering the relaxation commented in (3.6) and introducing the objective function k_m as an additional optimization variable.

Remark 3.1. Constraint (3.7b) consists of two (real and imaginary parts of the determinant) nonlinear equality constraints in the variables X. By using Laplace expansion of the determinant [1] and the fact that Δ is structured, an analytical expression for the gradient of (3.7b) with respect to δ and x can be obtained and provided to the optimizer. As for ω, this is more tedious and therefore finite differences are employed.

Note also that, from a continuation perspective, (3.7b) can be regarded as an analog of the real scalar test functions commonly used to detect Hopf bifurcations [3]. The latter can be efficiently formulated by means of bordered matrices techniques and have the property that the test function has a zero at a bifurcation point. The main difference here is that (3.7b) is complex, thus consists of two real scalar equations. This is due to the fact that the frequency ω of the purely imaginary eigenvalues appear explicitly in the constraint (and thus is an additional independent variable), which is different from the test functions formulation. This is an important feature of the developed approach, and possible ways to exploit it will be discussed later.

Enforcing the transversality condition

Program 3.2 allows worst-case perturbations to be computed such that the Jacobian of $\tilde{f}$ linearized around the perturbed equilibrium point has a pair of purely imaginary eigenvalues. This, however, does not guarantee that the perturbed system undergoes a Hopf bifurcation because transversality (Condition 2 of Theorem 2.1) is not automatically verified. Constraints guaranteeing that transversality is satisfied can be appended to (3.7) in different ways, including using test functions [3] or automatic differentiation [23]. Here an approach leveraging the versatility of the LFT paradigm is proposed. Consider a small fixed constant ϵ_p which defines the perturbed bifurcation parameter $\bar{p}_{\epsilon_p} = (1+\epsilon_p)\bar{p}_0$. The LFT $\mathcal{F}(M^{\epsilon}_{\tilde{J}}, \Delta^{\epsilon})$ of the Jacobian at $\bar{p}_{\epsilon_p}$ can be written following (3.4) as

$$\mathcal{F}(M^{\epsilon}_{\tilde{J}}, \Delta^{\epsilon}) = \mathcal{F}(\mathcal{F}(\mathcal{F}(M^{\epsilon}_{\tilde{J}}, \Delta^{\epsilon}_{\nu}), \Delta^{\epsilon}_{x}), \Delta_u), \tag{3.8a}$$

$$\Delta^{\epsilon} = \mathrm{diag}(\Delta_u, \Delta^{\epsilon}_{x}, \Delta^{\epsilon}_{\nu}), \quad M^{\epsilon}_{\tilde{J}} = \left[M^{\epsilon}_{\tilde{J}_{11}} M^{\epsilon}_{\tilde{J}_{12}}, M^{\epsilon}_{\tilde{J}_{21}} M^{\epsilon}_{\tilde{J}_{22}}\right], \tag{3.8b}$$

$$\Delta^{\epsilon}_{x} = \mathrm{diag}((1+\epsilon_x)x_1 I_{x_1}, ..., (1+\epsilon_x)x_j I_{x_j}, ..., (1+\epsilon_x)x_{n_x} I_{k_{n_x}}), \tag{3.8c}$$

$$\Delta^{\epsilon}_{\nu} = \frac{1}{\nu^{\epsilon}} I_{n_x}, \quad \nu^{\epsilon} = \epsilon_{\nu} + (1+\epsilon_{\omega})\omega, \tag{3.8d}$$

where ϵ_ν, ϵ_x, and ϵ_ω are unknown scalars described later. The following optimization problem is then proposed to determine the worst-case perturbation for which both conditions of the Hopf theorem are guaranteed to hold, that is, to calculate the margins to the closest Hopf bifurcation point.

PROGRAM 3.3.

$$\min_{X} k_m \quad \text{such that} \begin{cases} \tilde{f}(x, \bar{p}_0, \delta) = 0, & \text{(3.9a)} \\ \det(I - M_{\tilde{J}\,11}\Delta) = 0, & \text{(3.9b)} \\ -k_m \le \delta_i \le k_m, & \text{(3.9c)} \\ \tilde{f}((1+\epsilon_x)x, \bar{p}_{\epsilon_p}, \delta) = 0, & \text{(3.9d)} \\ \det(I - M^{\epsilon}_{\tilde{J}\,11}\Delta^{\epsilon}) = 0, & \text{(3.9e)} \end{cases}$$

$$X = [x; \delta; \omega; \epsilon_\nu; \epsilon_x; \epsilon_\omega], \quad n_{ctrs} = n_x + 2 + n_\delta + n_x + 2.$$

The first set of constraints (3.9a-3.9c) is identical to those in Program 3.2. The constraints (3.9d-3.9e) instead ensure that the Jacobian linearized at $\bar{p}_{\epsilon_p}$ has an eigenvalue ν^ϵ with real part ϵ_ν (3.8d). Making use of a finite difference approximation, it follows from the definition in (2.2) that $l_0 = \frac{\epsilon_\nu}{\epsilon_p}$. Therefore, existence of a solution to Program 3.3 with $\hat{\epsilon}_\nu \neq 0$ guarantees a Hopf bifurcation for the system.

Underlying Program 3.3 there is a perturbation argument which builds on the application of the IFT to the states x and the eigenvalue ν of the vector field $\tilde{f}(x, p, \hat{\delta})$ for fixed $\hat{\delta}$ and p in a neighbourhood of $\bar{p}_0$. Indeed, at $p = \bar{p}_0$, it holds $x = \hat{x}$ and $\nu = i\hat{\omega}$ for the constraints (3.9a-3.9c). When perturbing p by a small increment ϵ_p, a first order approximation for x and ν is assumed, and reflected in the choice of the scalars ϵ_x (3.8c), as well as ϵ_ω and ϵ_ν (3.8d). A vector ϵ_x, with an element for each component of x, could also be considered, by adding $n_x - 1$ unknowns to Program 3.3.

Remark 3.2. Program 3.2 does not mathematically guarantee the onset of a Hopf bifurcation because it does not take into account the transversality condition, and for this reason Program 3.3 is proposed. However, for engineering systems where p has a physical meaning (e.g., load power in a power system, speed for an aircraft) the transversality condition is often automatically verified. In fact, cases where this condition is not satisfied are termed *degenerate* in the literature [18]. For this reason, the problem was stated in Sec. 3.1 assuming that the nominal system has a bifurcation at p_H whereas for $p = \bar{p}_0$ the system has a stable equilibrium. It is thus implicit in the formulation of the problem that a change of p has an effect on the stability of the system. In particular, it is expected that the critical eigenvalues of the perturbed Jacobian will cross the imaginary axis as p is perturbed around $\bar{p}_0$.

It is observed that, compared to Program 3.2, Program 3.3 only adds three unknowns to the vector of optimization variables X, and has $n_x + 2$ additional constraints. Its effect in terms of computational cost is thus not expected to be important. However, a strong reason to resort to Program 3.2 whenever possible is related to the local optimality of the solutions of nonlinear programs. This issue will be further discussed in Sec. 3.3, but it is remarked here that the addition of the constraints (3.9d-3.9e) has a detrimental effect on it. Indeed it is always advisable in nonlinear optimization to avoid redundant constraints in order to reduce the likelihood of local optima [33]. Based on these considerations, and the discussion in Remark 3.2, the proposed strategy is to employ Program 3.2 to find robust bifurcation margins and, if continuation analyses of the perturbed system show that the transversality condition is not fulfilled, use Program 3.3. It is noted that none of the analyses done in support of this study required the adoption of Program 3.3 (which however was tested to verify its soundness). For this reason, and also for the sake of clarity, in the remainder of the work Program 3.2 will be considered as the basis for discussion and further algorithms.

Specifying the type of closest Hopf bifurcation

The robust bifurcation margin k_m has been associated so far with the occurrence of a generic Hopf bifurcation. Attention is now focused on the nature of the bifurcation, i.e., subcritical or supercritical. The idea is to add a condition on the sign of the Lyapunov coefficient l_1 to the constraints of Program 3.2. This can be done by using the definition of l_1 (2.4), which requires the computation of left and right eigenvectors associated with the critical eigenvalue, and the tensors of second and third order derivative. By exploiting the fact that ω is an optimization variable, the eigenvectors can be computed without performing an eigenvalue analysis, but by direct computation as follows

$$(3.10)\qquad \begin{aligned} &(\tilde{J} - i\omega I_{n_x})q = 0, \quad q = [1; q_l],\\ &(\tilde{J}^T + i\omega I_{n_x})r = 0, \quad r = [1; r_l],\\ &\langle r, q\rangle = 1, \end{aligned}$$

where without loss of generality the first element of the eigenvectors has been fixed to 1. As for the tensors, the derivatives in (2.6) can be computed analytically in simple cases and by automatic or symbolic differentiation for more complex ones. Alternatively, in [27] efficient strategies to avoid computing second and third order derivatives of the vector field are discussed. In any case, they are available as a function of the optimization variables x and δ, and thus the only addition to the vector of unknowns X is essentially l_1.

In conclusion, given a positive tolerance ϵ_l on the value of the Lyapunov coefficient, and an integer $s_l = \pm 1$ defining the sign of l_1 ($s_l = 1$ for subcritical and $s_l = -1$ for supercritical), the following program allows the closest subcritical or supercritical Hopf bifurcation to be computed.

PROGRAM 3.4.

$$\min_X k_m \quad \text{such that} \begin{cases} \tilde{f}(x, \bar{p}_0, \delta) = 0, & (3.11a)\\ \det(I - M_{\tilde{J}\,11}\Delta) = 0, & (3.11b)\\ -k_m \le \delta_i \le k_m, \qquad i = 1, ..., n_\delta, & (3.11c)\\ s_l l_1 - \epsilon_l > 0, & (3.11d) \end{cases}$$

$$X = [x; \delta; \omega; l_1], \quad n_{ctrs} = n_x + 2 + n_\delta + 1.$$

To summarize the content of this Section, the problem of computing the closest Hopf bifurcation point in the uncertain parameter space has been formulated via a nonlinear optimization problem and has been presented incrementally in order to stress the key steps involved. Because the Hopf bifurcation can be of two types, namely subcritical and supercritical, two Programs are proposed. Program 3.2 determines the closest Hopf bifurcation to a given stable equilibrium (this might be subcritical or supercritical, depending on the specific case), whereas Program 3.4 allows the type of closest Hopf bifurcation (via a constraint on the Lyapunov coefficient) to be specified.

3.3. Continuation-based multi-start strategy. The programs discussed in Section 3.2 allow margins to Hopf bifurcation for a nominally stable equilibrium point in the face of uncertainties to be computed. The main issue with this approach is that, due to the fact that is based on nonlinear optimization, there is no guarantee that the one found is the closest bifurcation, and thus in practice only upper bounds on k_m are computed. In other words, global minima might be missed and thus there could be a vector $\bar{\delta}$ featuring a smaller norm than $\hat{\delta}$ which causes a Hopf bifurcation. Local optima are a well known issue in nonlinear optimization and, while there exist global optimization algorithms that can guarantee global optima, their computational burden grows exponentially with the dimension of the problem and thus often are not practical solutions [33].

Mitigation strategies when local solvers (e.g. interior point methods) are used depend on several aspects, including specific features of the program (e.g., objective functions) and adopted optimization algorithms [17]. For this problem the objective is to compute worst-case perturbations quantified by means of a scalar metric, thus a possible way to account for this issue is to estimate a guaranteed smallest magnitude of the perturbation for which the system is stable. This is the approach taken in μ analysis, where the computation of μ_{LB} is known to be prone to local minima and as a remedy upper bounds μ_{UB} have been proposed. Lower bounds on k_m (nonlinear analogs of μ_{UB}) could then be a strategy in the present context, but this has not been pursued here and could be a topic of future research.

As for the optimization algorithms, the focus of this work is not on developing ad-hoc advanced optimization strategies, hence off-the-shelf algorithms available in MATLAB for nonlinear constrained problems are employed [31]: These include: *interior point*, which solves the constrained problem using a sequence of unconstrained optimizations by using barrier or penalty functions to account for the constraints; *active set* and *sqp*, belonging to the class of sequential quadratic programmes, which directly solve the constrained problem via a series of approximating quadratic programming based on the Karush-Kuhn-Tucker equations (necessary conditions for optimality of constrained optimization problems). Leveraging the availability of solvers based on different optimization methods, a (naive but possible) strategy employed in the work is to restart the programs using different solvers.

Another good practice to reduce the likelihood of local minima is to formulate the problem in the *simplest* way possible [33], e.g., using smooth objective functions and constraints and avoiding redundant constraints. These two principles have guided the idea of introducing the objective function k_m to relax the non-smooth bound on the uncertainty set involving $\bar{\sigma}$, which lead to the equivalent constraints (3.6). Moreover, the aim of simplifying as much as possible the set of constraints prompted the discussion in Remark 3.2, where it was proposed (based on a physically motivated assumption) to resort to Program 3.3 only if the solution does not satisfy the transversality condition.

A strategy which exploits a distinctive feature of this formulation is to run Program 3.2 at a given frequency, i.e., ω does not belong to X but is fixed a priori. The rationale behind this is twofold. From a mathematical point of view, the optimization is simplified by the fact that constraint (3.7b) does not depend on the frequency and this enhances the accuracy of the result. From a bifurcation perspective, fixing the frequency restricts the mechanisms by which the system can undergo a Hopf bifurcation when subject to uncertainties, which reduces the number of feasible solutions in the first place, and as a result makes it also more likely to detect the optimal one. A value of k_m can be associated with each discrete frequency, and the smallest of these values can be regarded as the most critical. A natural drawback of this approach is that critical frequencies can be missed, but this can be overcome by running Program 3.2 in a second step with ω as optimization variable and initializing it with values corresponding to the critical solution.

Despite these measures, the risk of falling into local minima is still present. In particular, the programs' initialization represents a critical aspect and thus a continuation-based multi-start strategy is proposed. Assume that the optimizer has found a solution $\hat{X}$ to Program 3.2. The goal is then to provide the optimizer with a set of initializations, derived from $\hat{X}$ but possibly not leading the optimizer to find the same solution, which allows an exhaustive optimization campaign to be performed. The following extended continuation problem based on the constraints of Program 3.2

is first considered

$$F(x, \delta, \omega, \lambda_d, \lambda_k) = \begin{pmatrix} \tilde{f}(x, \bar{p}_0, \delta) \\ \det(I - M_{\tilde{J}\,11}\Delta) \\ \bar{\sigma}(\Delta_u) \end{pmatrix} - \begin{pmatrix} 0 \\ \lambda_d \\ \lambda_k \end{pmatrix} = 0. \tag{3.12}$$

This can be recast in the formalism of (2.7) by setting

$$\begin{aligned} &u = X = [x; \delta; \omega],\ u \in \mathbb{R}^{n_u},\ n_u = n_x + n_\delta + 1, \\ &\lambda = [\lambda_d; \lambda_k],\ \lambda_d \in \mathbb{R}^2,\ \lambda_k \in \mathbb{R}^1, \\ &\Phi = \tilde{f}(x, \bar{p}_0, \delta),\ \Phi : \mathbb{R}^{n_u} \to \mathbb{R}^{n_x}, \\ &\Psi = [\det(I - M_{\tilde{J}\,11}\Delta), \bar{\sigma}(\Delta_u)],\ \Psi : \mathbb{R}^{n_u} \to \mathbb{R}^3, \\ &F : \mathbb{R}^{n_x + n_\delta + 3} \to \mathbb{R}^{n_x + 3}. \end{aligned} \tag{3.13}$$

Let $\mathbb{I} = \{1, 2\}$ and $\bar{\mathbb{I}} = \{3\}$ be its complement, with $\lambda_{\mathbb{I}} = \{\lambda_i | i \in \mathbb{I}\}$ and $\lambda_{\bar{\mathbb{I}}} = \{\lambda_i | i \in \bar{\mathbb{I}}\}$, and $u^* = \hat{X}$, $\lambda^* = \Psi(u^*)$. By construction, the restriction $F(u^*, \lambda)|_{\lambda_{\mathbb{I}} = \lambda^*_{\bar{\mathbb{I}}}} = 0$ and $F(u, \lambda)|_{\lambda_{\mathbb{I}} = \lambda^*_{\bar{\mathbb{I}}}}$ satisfies the IFT at (u^*, λ^*). Therefore, $F(u, \lambda)|_{\lambda_{\mathbb{I}} = \lambda^*_{\bar{\mathbb{I}}}}$ defines a continuation problem for the d-manifold with $d = n_x + n_\delta + 1 - (n_x + 2) = n_\delta - 1$. Note that $\lambda_{\mathbb{I}}$ (coinciding with λ_d) are inactive continuation parameters (corresponding to active constraints) because they are kept constant during continuation and they ensure the singularity of the LFT $\mathcal{F}(M_{\tilde{J}}, \Delta)$. Since $\lambda^*_d = 0$, the corresponding active constraints could have been equivalently embedded in the zero function Φ but, for consistency with the parallel between f and Φ discussed in Sec. 2.1.2, this has been used for the vector field only. On the other hand, $\lambda^*_{\bar{\mathbb{I}}}$ (i.e., λ_k) corresponds to an inactive monitor function bookkeeping the magnitude of the perturbation at each step of the continuation.

The manifold associated with (3.12), denoted here by $\mathcal{H}$, represents the set of Hopf bifurcation points *connected* to the solution $\hat{X}$ in the uncertain parameter space. A first important observation is that the dimension of $\mathcal{H}$ is $n_\delta - 1$. This is in agreement with the well known fact [3] that a branch (i.e., 1-dimensional manifold) of Hopf points can be obtained by continuing simultaneously two parameters starting from a known initial point. Indeed, in the case of two uncertainties ($n_\delta = 2$) $\mathcal{H}$ is the branch of Hopf points connected to the initial solution $\hat{X}$.

In principle, the computation of $\mathcal{H}$ could directly locate bifurcation points associated with perturbations featuring a smaller magnitude than $\hat{\delta}$ by monitoring λ_k (note however that they could still be local optima since only the connected branches can be tracked). In addition to that, exploring the *surroundings* of $\hat{X}$ (using a continuation meaning of this terminology) can provide the sought initialization points for a new optimization campaign. Unfortunately, $\mathcal{H}$ is generally multidimensional. In fact, it is reasonable to assume that even for a relatively small number of uncertainties computing $\mathcal{H}$ is not viable. To overcome this, a 1-dimensional restriction of $\mathcal{H}$ is constructed by considering a parametrization of the uncertainty set δ with a vector function $g(z, y) : \mathbb{R}^2 \to \mathbb{R}^{n_\delta}$, where the 2 independent variables z and y have been introduced. The definition of g is arbitrary and various strategies can be pursued. The approach taken here assumes that two solutions $\hat{X}^1$, and $\hat{X}^2$ from Program 3.2 are available (their selection will be commented on later). Given the associated perturbation vectors $\hat{\delta}^1$, and $\hat{\delta}^2 \in \mathbb{R}^{n_\delta}$, a possible choice for g is then

$$(3.14) \qquad g(z,y) : \mathbb{R}^2 \to \mathbb{R}^{n_\delta} \begin{cases} \hat{\delta}^1_1 z + \hat{\delta}^2_1 (1-y), \\ ... \\ \hat{\delta}^1_i z + \hat{\delta}^2_i (1-y), \\ ... \\ \hat{\delta}^1_{n_\delta} z + \hat{\delta}^2_{n_\delta} (1-y), \end{cases}$$

Note that by construction $g(1,1) = \hat{\delta}^1$ and $g(0,0) = \hat{\delta}^2$.

Based on this, the following continuation problem is formulated

$$(3.15) \qquad F(x,\delta,\omega,z,y,\lambda_d,\lambda_k,\lambda_g) = \begin{pmatrix} \tilde{f}(x,\bar{p}_0,\delta) \\ \det(I - M_{\tilde{J}\,11}\Delta) \\ \bar{\sigma}(\Delta_u) \\ \delta - g(z,y) \end{pmatrix} - \begin{pmatrix} 0 \\ \lambda_d \\ \lambda_k \\ \lambda_g \end{pmatrix} = 0.$$

With respect to the definitions in (3.13), z and y have been added to the vector of continuation variables u (i.e., $u = [X; z; y]$), while the vector function $\delta - g$ has been added to the family of monitor functions Ψ (with associated continuation parameters $\lambda_g \in \mathbb{R}^{n_\delta}$).

Let $\mathbb{I} = \{1, 2, 4, ..., 4 + n_\delta\}$, and $\bar{\mathbb{I}}$, $\lambda_{\mathbb{I}}$, $\lambda_{\bar{\mathbb{I}}}$ as before. Two starting points are available, respectively $u^* = [\hat{X}^1; 1; 1]$ and $u^* = [\hat{X}^2; 0; 0]$, with $\lambda^* = \Psi(u^*)$. Note that in both cases $\lambda^*_g = \Psi(u^*) = 0$ by construction. Therefore, $\delta = g(z,y)$ at each step of the continuation, and δ is expressed as a linear combination of $\hat{\delta}^1$ and $\hat{\delta}^2$.

Since $F(u^*,\lambda)|_{\lambda_{\mathbb{I}} = \lambda^*_{\mathbb{I}}} = 0$ and $F(u,\lambda)|_{\lambda_{\mathbb{I}} = \lambda^*_{\mathbb{I}}}$ satisfies the IFT at (u^*, λ^*), then a manifold $\mathcal{H}_g$ with dimension $d = n_x + n_\delta + 3 - (n_x + 2 + n_\delta) = 1$ is defined. Crucially, the dimension is 1 irrespective of the number of uncertainties n_δ, with the drawback that these are now constrained to vary according to (3.14). $\mathcal{H}^1_g$ and $\mathcal{H}^2_g$ indicate the manifold built starting from $[\hat{X}^1; 1; 1]$ and $[\hat{X}^2; 0; 0]$ respectively, with the subscript and the superscript highlighting the dependence on the parametrization of the uncertainties g and the initial point.

The construction of $\mathcal{H}_g$ requires two perturbation vectors $\hat{\delta}^1$ and $\hat{\delta}^2$. This is not restrictive, since as a result of the local optimality typically more than one solution is available. In addition, the possibility of running the optimization at a fixed frequency ω can be advantageously exploited with the goal of obtaining different *modes* of perturbations. Indeed, as discussed before, Hopf bifurcations occurring at different frequencies could represent different mechanisms underlying the loss of stability, thus considering a linear combination of the perturbations as in (3.14) represent an efficient strategy to select points on $\mathcal{H}_g$.

To sum up the multi-start strategy approach, the starting point is Program 3.2 which provides a solution consisting of an equilibrium point $\hat{x}$ of $\tilde{f}$ perturbed by $\hat{\delta}$ such that the associated Jacobian $\tilde{J}$ has a pair of purely imaginary eigenvalues. This is not necessarily the closest bifurcation point to the nominal system due to the possibility of local minima. However, $\hat{X}$ can be used to compute the restricted manifold $\mathcal{H}_g$ via a numerically *cheap* continuation problem once a parametrization g for the uncertainty set is provided. Continuation of $\mathcal{H}_g$ has two objectives. First, it could directly detect improved solutions of Program 3.2 (if $\lambda_k < \hat{k}_m$). Second, points on $\mathcal{H}_g$ can be used to run Program 3.2 with different initializations.

If the manifold $\mathcal{H}_g$ gathers a large number of points, and running the optimization for each of them is not viable, criteria could be employed to select a subset of them only. Keeping in mind that the goal is to provide initializations which possibly make the optimizer converge to different points from the initial solution $\hat{X}$, the premise of these criteria is to detect on $\mathcal{H}_g$ perturbation vectors *qualitatively* different from $\hat{\delta}$. Possible indicators are for example the frequency ω and the changes in sign of the parameters in δ (recall that these are normalized, thus a change in sign reveals a change in the direction of perturbation for the considered parameter).

3.4. Comparison with the direct method. The framework presented in the previous sections allows the computation of the robust bifurcation margin k_m via nonlinear optimization (section 3.2) aided by a multi-start strategy (3.3). Despite its importance for the analysis of nonlinear systems, the computation of the closest Hopf bifurcation point to a stable equilibrium in the uncertain parameter space has not been adequately investigated so far. The only alternative approach available in the literature is the so-called *direct* method [12], and the objective of this section is to point out the differences (and the associated advantages) of the formulation proposed in this paper (in the remainder of this section termed *margin* method) with respect to it.

The direct method for Hopf bifurcations considers as starting point the vector field (2.1) where $n_p > 1$, i.e. the vector of bifurcation parameters is multidimensional. Given a vector $\bar{p}_0$ associated with a stable equilibrium, the closest point to $\bar{p}_0$ in the set of parameters (or hypersurface) Σ for which the equilibrium experiences a Hopf bifurcation is sought. A first difference is thus that in the margin method a distinction is drawn between bifurcation parameter p (of dimension equal to the codimension of the bifurcation, which is 1 for the Hopf case) and uncertain parameters δ, and the closest Hopf point is sought in the uncertainty space only (that is, $\bar{p}_0$ is fixed). Conversely, in the direct method bifurcation and uncertain parameters are all gathered in p and can all be perturbed in order to reach the closest bifurcation point. This difference only pertains to the formulation of the problem, but it is worth highlighting it since two different perturbation scenarios are effectively considered.

The key observation leveraged by the direct method is that if p_* is the closest point to $\bar{p}_0$ in Σ, then the vector $p_* - \bar{p}_0$ is parallel to the normal vector to the hypersurface Σ at p_*. Moreover, p_* is a *local* minimum if the distance $|p_* - \bar{p}_0|$ is smaller than the reciprocal of the curvature of Σ at p_*.

Implementation of these conditions lead to the extended system of equations defining a Hopf bifurcation ([12], Section 5). The name *extended* derives from the fact that, for $n_p = 1$, this set of equations reduces to the standard system of equations to compute Hopf bifurcation branches (Th. 2.1). The multidimensional case exploits the fact that the normal vector at p_* can be written out as a function of $\nabla_p f|_{p=p_*}$ and of the eigenvector of the Jacobian $\nabla_x f|_{p=p_*}$ associated with the purely imaginary eigenvalues. In turn, the curvature can be written as a function of the normal vector. Building on these relationships and enforcing all the associated constraints, the problem is finally formulated as the solution of $6n_x + n_p + 2$ nonlinear equations in $6n_x + n_p + 2$ unknowns. Similarly to the margin method (see the vector X in Program 3.2), the unknowns of the problem include the perturbed equilibrium (n_x), the closest bifurcation parameter vector (n_p), and the frequency (1). However, in addition to these there are another $5n_x + 1$ unknowns which are introduced in order to express the rest of the constraints, and clearly do not feature in the margin method. The key ideas leveraged by the margin method to avoid these additional constraints are to enforce the constraint on the Jacobian as singularity of the LFT (3.7b) and cast the minimum distance problem as maximum singular value minimzation of the perturbation matrix

Δ. As for the number of constraints, Program 3.2 has $n_{ctrs} = n_x + 2 + n_\delta$ while the direct method features $6n_x + n_p + 2$. A comparison in terms of size of the problem, both in terms of unknowns and constraints, points out an objective advantage of the margin method with respect to the direct method. Quoting the author in [12], *"this direct method for computing Hopf bifurcations may bee too cumbersome to be useful if n_x is large"*.

The distinctions between the two methods are however not restricted to the size of the problem. For example, the mathematical formulation of the problem is different. In the margin method, k_m is the result of an optimization problem whereas in the direct method a determined (the number of constraints equals the number of unknowns) set of nonlinear equations has to be solved (e.g. with Newton-type methods). This is deemed an advantage of the margin method, since the greater degree of freedom in finding the solution can be exploited using optimization techniques in order to achieve higher efficiency in the computation and more robustness to the problem of local minima. As for the latter aspect, it is further observed that the margin method is also equipped with the multi-start strategy (3.3), as opposed to the direct method where there are no strategies to directly tackle the problem of converging to local minima.

Another favourable feature offered by the margin method is that it allows the type of closest bifurcation to be specified via constraint on the Lyapunov coefficient (Program 3.4). This is done in a relatively straightforward way by using the fact that ω is an optimization variable, and thus the eigenvectors needed for the computation of l_1 (2.4) are available without performing an eigenvalue analysis (3.10). As a result, Program 3.4 only adds one unknown (l_1) and one scalar constraint to Program 3.2 where the type of bifurcation is not specified. This is again due to the LFT formulation of the problem that provides an analytic dependence of the constraints on ω (see also Remark 3.1). Conversely, the option of specifying the closest bifurcation is not available in the direct method, nor is it clear how it could be added without incurring a further substantial increase in the number of unknowns and constraints.

Another important aspect is related to the type of constraints involved in the two problems. As discussed in Remark 3.1, the gradients of the constraints in Program 3.2 with respect to the unknowns (with the exception of ω, which is more tedious) can all be analytically computed and provided to the solver, with great advantage in terms of efficiency of computation. This clearly does not apply to the direct method due to the very complicated definition of the constraints (involving eigenvectors and their projections) and of the unknowns.

Finally, a unique feature of the robust bifurcation margin k_m owes to its interpretation as nonlinear extension of the structured singular value μ. This indeed opens up the possibility to transfer to the bifurcation field many of the well established approaches in robust control [48]. This applies to: modelling, where advanced LFT algorithms [28, 29] can be employed to efficiently formulate the constraints of Program 3.2 and Program 3.4; analysis, where the insightful interpretations of μ and associated analysis strategies (sensitivity, frequency-domain analysis) [26] carry over to k_m; and ultimately robust control design, whereby a (potentially nonlinear) controller is synthesised to prevent bifurcations in the face of a given uncertainty set. While examples of the first two aspects have been given throughout the section and will be exemplified further in section 4, the latter is an exciting prospective line of research that can build on this initial work.

4. Numerical examples.

The proposed concept of robust bifurcation margin is demonstrated on two test cases from the literature. The first is a power system model for which the sensitivity of the Hopf bifurcation to modeling parameters was considered in [13], while the second is an aeroelastic case study previously studied with linear robust control techniques in [25].

4.1. Power system.

4.1.1. Model description. The first example considers the single machine power load system with voltage regulator and dynamic load model studied in [13] and depicted in Fig. 4. The model used in [13] is very similar to the one originally proposed in [7], with the variations discussed next. The model in [7] consists of: five ordinary differential equations representing the dynamics of the generator voltages $E_d^{'}+jE_q^{'}$, the voltage regulator state R_f and output voltage V_R, and the field voltage E_{FD}; two algebraic equations which relate the load bus voltage phasor $V_L\underline{/\theta}$ to the voltage source $E_d^{'}+jE_s^{'}$ and the load demand P_L+jQ_L, where P_L and Q_L are respectively the constant (and fixed a priori) active and reactive power components. The goal of the regulator is to control the voltage E_s at the high side of the transformer given a reference voltage setpoint E_{ref}, which depends on the loading level.

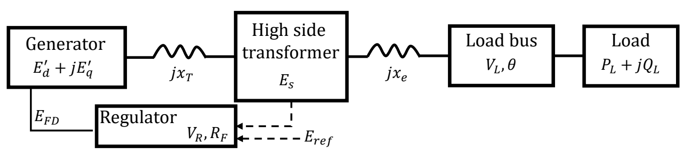

FIG. 4. *Power system sketch.*

Differently from [7], the model in reference [13] considers: a dynamic power load (i.e. P_L and Q_L are not constant); a setpoint E_{ref} which is fixed for all loading levels; and an expression of the voltage E_s as a function of the other state variables. Due to these changes, two ordinary differential equations are added for V_L and θ, and the two algebraic equations become explicit equations for P_L and Q_L.
The resulting set of seven ordinary differential equations describing the power system, with vector of states $x=[E_d^{'};E_q^{'};V_R;E_{FD};R_f;\theta;V_L]$, is:

$$T_{q0}^{'}\dot{E}_d^{'} = -E_d^{'} + (x_q - x_d^{'})I_q, \tag{4.1a}$$

$$T_{d0}^{'}\dot{E}_q^{'} = -E_q^{'} - (x_d - x_d^{'})I_d + E_{FD}, \tag{4.1b}$$

$$T_A\dot{V}_R = -V_R + K_A(E_{ref} - E_s - \frac{K_f E_{FD}}{T_f} + R_f), \tag{4.1c}$$

$$T_E\dot{E}_{FD} = -E_{FD} + V_R, \tag{4.1d}$$

$$T_f\dot{R}_f = -R_f + \frac{K_f E_{FD}}{T_f}, \tag{4.1e}$$

$$D\dot{\theta} = P_L - lPF, \tag{4.1f}$$

$$k\dot{V}_L = Q_L - l\sqrt{1-PF^2}. \tag{4.1g}$$

where: T_{q0} and T_{d0} are the open circuit time constants; x_d and x_q are the synchronous reactances; $x_d^{'}$ is the transient reactance; I_d and I_q are the currents; T_A and K_A are the voltage regulator time constant and gain; T_E is the exciter time constant; T_f and K_f are the time constant and gain of the feedback loop; D and k are time constants of the load dynamics; PF is the power factor and l parameterizes the increase of the

constant power part of the load (this will be used as bifurcation parameter in the analyses).
This set of equations must be closed with the defining equations for I_d, I_q, P_L, Q_L, and E_s. For the currents, the following holds [7]:

$$
\begin{aligned}
I_d &= \frac{1}{x_E}(E_q^{'} - V_L\cos(\delta-\theta)), \\
I_q &= \frac{1}{x_E}(-E_d^{'} + V_L\sin(\delta-\theta)), \\
x_E &= x_d^{'} + x_T + x_e.
\end{aligned} \tag{4.2}
$$

where δ is the rotor angle, x_T is the high side transformer reactance and x_e is the transmission line reactance.
The equations for the remaining three variables are not provided in [13]. The relationships for P_L and Q_L are derived here from the two aforementioned algebraic equations in [7], which now allow an explicit expression for the load components to be obtained since the phasor $V_L\underline{/\theta}$ has a dedicated dynamic description (4.1f-4.1g).
As for E_s, a relationship to the state variables is derived by considering the loadflow equation for the circuit with the voltage source at the high side of the transformer. This leads to:

$$
P_L = \frac{V_L}{x_E}\cos(\theta)\tilde{P} - \frac{V_L}{x_E}\sin(\theta)\tilde{Q}, \tag{4.3a}
$$

$$
Q_L = \frac{V_L}{x_E}\sin(\theta)\tilde{P} + \frac{V_L}{x_E}\cos(\theta)\tilde{Q}, \tag{4.3b}
$$

$$
\tilde{P} = -E_d^{'}\cos(\delta) + E_q^{'}\sin(\delta) - V_L\sin(\theta),
$$

$$
\tilde{Q} = E_d^{'}\sin(\delta) + E_q^{'}\cos(\delta) - V_L\cos(\theta),
$$

$$
E_s = \frac{1}{V_L}\sqrt{(x_eP_L)^2 + (x_eQ_L + V_L^2)^2}. \tag{4.3c}
$$

Note that the same expression for E_s was used in [46], where a very similar power system was analyzed.

Table 1 reports the values of the parameters used here for the power system model. These are all taken from [7], except for D and k (introduced anew in [13]) and K_f, whose value was changed in [13]. As for the rotor angle δ, it is noted that their dynamic is assumed faster than the dominant voltage dynamics, thus the angle is in quasi-steady state and does not have any effect on the results [7]. Time constants are in seconds, reactance are p.u. while all the other parameters are dimensionless.

TABLE 1
Power system model parameters.

x_T	x_e	x_d	x_q	$x_d^{'}$	$T_{d0}^{'}$	$T_{q0}^{'}$	K_A	T_A	T_E	K_f	T_f	PF	D	k
0.15	0.34	1	1	0.18	5	1.5	30	0.4	0.56	0.1	1.3	0.95	0.05	0.1

Numerical continuation is applied to the nominal model using the parameter l as bifurcation parameter. The (non-zero) stable equilibrium point at $l = 0$ is found by simulating the model and this is provided as an initialization to COCO. The branch of equilibrium points as l is increased is reported in Fig. 5 by showing the values of three components of the state vector, namely $E_d^{'}$, R_f, and V_L.

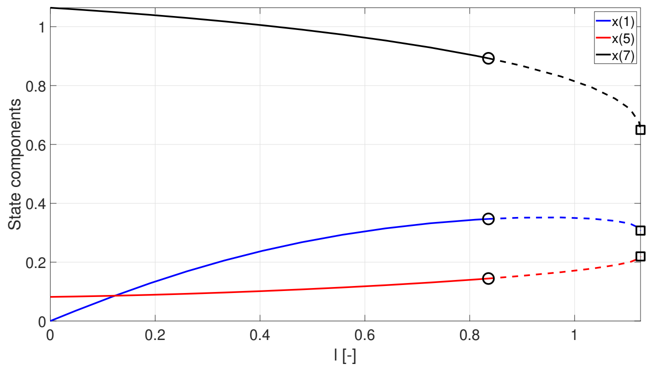

FIG. 5. *Bifurcation diagram for the nominal power system model.*

The analyses show that the system has a branch of stable equilibria for low values of l (this part of the branch is denoted by a solid line), which undergoes a Hopf bifurcation at l_H=0.83 (circle marker), with a frequency of the associated imaginary eigenvalues equal to ω_H=2.6 $\frac{rad}{s}$, and a saddle node bifurcation at l_{SN}=1.13 (square marker). As aforementioned, the model used in here is not exactly the same as that of [13] as insufficient information was provided in that reference to reproduce their results exactly. In [13], the Hopf bifurcation also occurred at a lower loading level than the saddle node one but at different values, i.e. l_H=0.37 and l_{SN}=1.03. Thus, qualitatively speaking, the results from Fig. 5 are similar to those in [13] (see also the sensitivity analysis discussed next) and should enable the proposed robust bifurcation margin approach to be tested by comparing with the results from [13][1].

4.1.2. Sensitivity analysis of the Hopf bifurcation. The authors in [13] compute the sensitivity of both bifurcations to the model's parameters (the focus will be here only on the analyses for the Hopf one). This computation is performed by first defining what is termed the *loading margin to instability* at l_0 (a value of the bifurcation parameter l corresponding to a stable equilibrium) as $M(l_0) = l_H - l_0$. The *first-order* sensitivity M_c of M to a generic parameter c (here c represents any model parameter, in the present case those in Table 1) is then computed as the partial derivative of M with respect to c evaluated at l_0, i.e. $M_c(l_0) = \frac{\partial M}{\partial c}\big|_{l=l_0}$. Its computation is performed using normal vectors to the manifold of Hopf bifurcation points and essentially consists of a sensitivity of the critical eigenvalue. An approximation to this sensitivity can be computed as $\tilde{M}_c = \frac{M(l_0,c+\epsilon)-M(l_0,c)}{\epsilon}$, where $M(l_0, c+\epsilon) = l_H^{c+\epsilon} - l_0$ and $l_H^{c+\epsilon}$ is the value of l at which a Hopf bifurcation occurs when the parameter c is increased to $c + \epsilon$. The quantity $\tilde{M}_c$ is thus a finite difference approximation of M_c and can be computed via numerical continuation. The results of such a sensitivity analysis are reported in Table 2 for the parameters previously listed in Table 1.

TABLE 2
Sensitivity of the Hopf bifurcation to model parameters (continuation-based).

	x_T	x_e	x_d	x_q	$x_d^{'}$	$T_{d0}^{'}$	$T_{q0}^{'}$	K_A	T_A	T_E	K_f	T_f	PF	D	k
$\tilde{M}_c$	-0.96	-1.3476	-0.05	-0.006	-0.9111	0.039	0.0047	0.003	-0.2975	-0.1982	2.1	-0.14	1.5	-0.005	0.11

[1]A MATLAB implementation of the power system model presented in this section, together with a file to run continuation analyses with COCO, is available at
https://github.com/AndreaIan/PowerSystem_cont

It is noted that the sign of all the sensitivities (a negative sign means that an increase of the parameter makes the loading margin to instability decrease) coincide with those reported in [13] except for k, and the magnitude (proportional to the sensitivity to that parameter) is also generally well captured.

In order to show the connection between the sensitivity approach used in [13] and the concept of robust bifurcation margin, a first type of analysis is discussed next. A set of four parameters from the power system model is considered, namely x_q, K_A, T_A, and K_f. Without loss of generality, only a subset of the parameters in Table 2 is selected to allow a more clear interpretation of the results. A subcritical value of the loading level at which robustness of the plant is studied is then selected; this is denoted $\bar{l}_0$ according to the notation adopted in section 3.1. In all the analyses presented here the value $\bar{l}_0 = 0.725 < l_H$ will be considered. Once the set of uncertain parameters and a value of the bifurcation parameter is selected, the corresponding LFT can be constructed. It is observed that the dependence of the vector field on the states cannot be captured directly in an LFT fashion. This is due to the trigonometric functions (4.2-4.3a-4.3b) and square root (4.3c). For this reason, Taylor expansions of these functions about the equilibrium state at $\bar{l}_0$ are considered. The order of the expansion (1 and 2 depending on the specific state) is selected in order to guarantee a satisfactory trade-off between accuracy and size of the LFT $\mathcal{F}(M_{\tilde{J}}, \Delta)$. For all the uncertain parameters a range of variation of $\pm 15\%$ from the nominal value is considered.

Program 3.2 is employed with an initialization provided by the nominal values of the equilibrium point and of the uncertainties. The value of the Lyapunov coefficient l_1 will not be considered as a variable in these analyses since the goal is not to study the effect of the parameters on the type of Hopf bifurcation, even though this would also be possible within this framework. Five different tests will be considered: four in which only one parameter belongs to the uncertainty set Δ_u (the total size of each of the four LFTs is 17), and one in which all the four parameters are included in Δ_u (the total size of the LFT is 25). The results are reported in Table 3 in terms of robust stability margin k_m, frequency $\hat{\omega}$ and worst-case perturbation for the normalized uncertainties.

TABLE 3
Sensitivity analysis with the robust bifurcation margin at $\bar{l}_0 = 0.725$.

test	k_m	$\hat{\omega}$ $\frac{rad}{s}$	δ_{x_q}	δ_{K_A}	δ_{T_A}	δ_{K_f}
1	24.3	2.3	24.3	·	·	·
2	∞	n.a.	·	n.a.	·	·
3	7.8	2.1	·	·	7.8	·
4	2.5	2.6	·	·	·	-2.5
5	1.54	2.2	1.54	-1.54	1.54	-1.54

The value of k_m for the first four tests, where only one parameter at a time is allowed to vary, can be considered as a measure of the sensitivity of the Hopf bifurcation to that parameter –and it is thus expected to show similar results to those obtained in [13]. Indeed, all the predictions reported in Table 2 (which was in agreement with [13]) are confirmed: high sensitivity to K_f, medium sensitivity to T_A, and practically no sensitivity to x_q and K_A (note that for the latter the optimization problem was found infeasible). Moreover, the signs of the worst-case perturbations are also in agreement with the findings in Table 2. The fifth test shows that when all the parameters are acting together the margin k_m decreases, but it is still greater than 1, that is the power system at $\bar{l}_0$ is robust to the uncertainty considered. For the predicted worst-case perturbation, the Hopf bifurcation taking place at $\bar{l}_0$ is associated with a frequency $\hat{\omega} = 2.2\frac{rad}{s}$ (recall that this is one of the optimization variables of Program 3.2), which is smaller than the one in the nominal case, but within the same frequency range.

While the proposed robust bifurcation margin framework can be used to retrieve the results of the sensitivity tests performed in [13], one of its advantage is that allows also for another type of sensitivity analysis. In particular, the effect of a parameter on the bifurcation is evaluated while simultaneously accounting for the other uncertainties affecting the system. This is inherently different from the sensitivity measure proposed in [13], which is a first-order approximation of the partial derivative of the margin, and thus effectively neglects any coupling among the uncertainties. This key aspect will be exemplified with a second type of k_m-based analysis.

It is known that the structured singular value μ can be used to evaluate the sensitivity of an instability to a set of n_δ selected parameters by performing multiple μ tests. This can be achieved for example using the skew-μ concept [30], or, within standard μ analysis tools, by considering two different uncertainty levels w_{1,d_i} and w_{2,d_i} (recall the definition of the uncertainty level in Eq. 3.3) for each parameter d_i ($i = 1, ...n_\delta$). In the first μ test (termed *base* to indicate it is the baseline test), all the parameters have the uncertainty level w_{1,d_i}, while in the following n_δ tests, the uncertainty level of the i-th parameter is set to w_{2,d_i} and for all the others it is kept at w_{1,d_j} (with $j \neq i$). The difference between the peak of the baseline μ plot and the peaks of the other n_δ tests is proportional to the sensitivity of the instability to the considered parameter. See [26] for an application of this analysis approach to the robust flutter problem.

In the same spirit, the parameters studied in Table 3 are analyzed here considering $w_1 = 0.15$ (i.e the previously defined 15% uncertainty range) and $w_2 = 0.3$ (i.e. doubling the range for the specific parameter used in the n_δ test). Program 3.2 is again employed and the results are shown in Table 4 (the first column identifies the test performed, i.e. *base* and then the parameter whose uncertainty level is set to w_2).

TABLE 4
Robust bifurcation margin sensitivity analysis at $\bar{l}_0 = 0.725$.

test	k_m	$\hat{\omega}$ $\frac{rad}{s}$	δ_{x_q}	δ_{K_A}	δ_{T_A}	δ_{K_f}
base	1.54	2.2	1.54	-1.54	1.54	-1.54
x_q	1.41	2.2	1.41	-1.41	1.41	-1.54
K_A	1.31	2	1.31	-1.31	1.31	-1.31
T_A	1.24	2.2	1.24	-1.24	1.24	-1.24
K_f	0.97	2.4	0.97	-0.97	0.97	-0.97

The baseline test coincides with test 5 in Table 3 but is reported to facilitate the comparison. The different sensitivity of the considered parameters is confirmed in this new analysis (from the least sensitive parameter x_q to the most sensitive one K_f). However, it is also clear that every parameter now has an effect on the shift of the bifurcation point towards $\bar{l}_0$. This is clearly seen comparing Table 3 and 4, where for the former table only K_f showed a high sensitivity effect (close to the value of the baseline test), but as shown in Table 4, when the uncertainty coupling is taken into account for the analysis, then all of the four parameters have similar levels to the baseline case. This finding results from taking into account perturbations in the other parameters while computing the parameter's sensitivity, and shows that the coupling among the uncertainties (not captured with first-order sensitivity approaches) can drastically affect the importance of some parameters. Specifically, parameters deemed unimportant with a first-order analysis can instead have a non-negligible impact on the bifurcation point.

To further characterize this aspect, Figure 6 depicts the reciprocal of the robust bifurcation margin k_m as a function of the frequency. The five curves represent the five cases considered in Table 4 and, unlike the *one-shot* tests discussed therein, are obtained by fixing the frequency in the optimization and computing the value of the margin at each frequency.

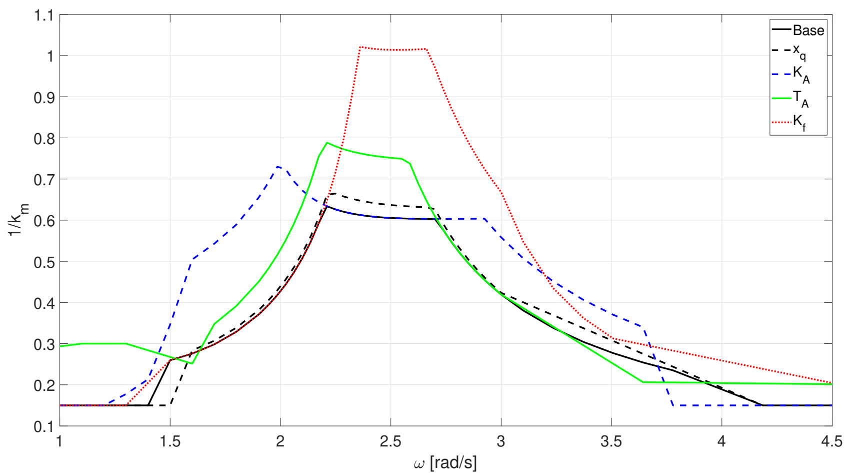

FIG. 6. *Sensitivity analysis of four parameters based on the robust bifurcation margin.*

The curves in Figure 6 resemble those typically employed in linear robust analysis with μ [48, 2, 26]. This points out once again the connection between the proposed concept of robust bifurcation margin k_m and the structured singular value μ. In particular, when $\frac{1}{k_m} \geq 1$, a perturbation in the allowed range of uncertainties exists such that a Hopf bifurcation is experienced by the system when perturbed. Note that the peak of each curve coincides with the reciprocal of the margin reported in Table 4. This representation allows the different sensitivities to the parameters discussed previously to be immediately inferred.

4.2. Aeroelastic system.

4.2.1. Model description. The typical section is an aeroelastic case study commonly used for flutter analysis purposes [4], and consists of a rigid airfoil with lumped springs simulating the 3 structural degrees of freedom (DOFs): plunge h, pitch α and trailing edge flap β. By defining the vector of structural states $x_s = [\frac{h}{b}; \alpha; \beta]$ and aerodynamic states x_a (used to capture the unsteady aerodynamic contribution), the system can be described in matrix form as:

$$\dot{x} = \begin{bmatrix} \dot{x}_s \\ \ddot{x}_s \\ \dot{x}_a \end{bmatrix} = \begin{bmatrix} 0 & I & 0 \\ -M^{-1}K & -M^{-1}B & M^{-1}D \\ 0 & E & R \end{bmatrix} \begin{bmatrix} x_s \\ \dot{x}_s \\ x_a \end{bmatrix} = \mathcal{A}x, \tag{4.4}$$

where M, B and K are respectively the aeroelastic inertial, damping and stiffness matrices:

$$
\begin{aligned}
M &= M_s - \frac{1}{2}\rho_\infty b^2 A_2, \\
B &= -\frac{1}{2}\rho_\infty b V A_1, \\
K &= K_s - \frac{1}{2}\rho_\infty V^2 A_0.
\end{aligned}
\tag{4.5}
$$

They include the structural mass M_s and stiffness matrices K_s plus the aerodynamic quasi-steady matrices A_i (ρ_∞ is the air density and b the half chord distance). D, E, and R in (4.4) come from the rational approximation of the unsteady aerodynamic operator. The parameters defining the model are provided in [25] and the total state size n_x is 9 (6 structural and 3 aerodynamic). The interested reader is referred to [25] for a complete definition of the parameters defining the model and further details on aeroelastic modeling with uncertainties.

Nonlinearities in K_s are considered in this work. Specifically, hardening cubic terms for the plunge and pitch degrees of freedom are assumed, and the matrix K_s is rewritten accordingly:

$$
K_s = K_s^L + K_s^{NL} = \begin{bmatrix} K_h^L & 0 & 0 \\ 0 & K_\alpha^L & 0 \\ 0 & 0 & K_\beta \end{bmatrix} + \begin{bmatrix} K_h^{NL} K_h^L \left(\frac{h}{b}\right)^2 & 0 & 0 \\ 0 & K_\alpha^{NL} K_\alpha^L \alpha^2 & 0 \\ 0 & 0 & 0 \end{bmatrix},
\tag{4.6}
$$

where K_h, K_α and K_β are respectively the plunge, pitch and control surface stiffness. As is common practice [11], the coefficients of the nonlinear terms are assumed proportional to the corresponding linear ones through the dimensionless coefficients K_h^{NL} and K_α^{NL} (assumed here equal to 100). The hardening effect modelled in (4.6) takes into account the fact that the stiffness properties change when the system undergoes large deformations, with an increase in the stiffness generally observed.

The dynamics of the system is thus in the form of the generic vector field (2.1), and, by selecting the speed V as bifurcation parameter, it holds:

$$
\begin{aligned}
\dot{x} &= f(x, V) = \mathcal{A}^L(V)x + f^{NL}(x), \\
J(x, V) &= \mathcal{A}^L(V) + \nabla_x f^{NL}(x),
\end{aligned}
\tag{4.7}
$$

where: $\mathcal{A}^L : \mathbb{R} \to \mathbb{R}^{n_x \times n_x}$ is obtained from $\mathcal{A}$ (4.4) by setting the nonlinear terms to zero; $f^{NL} : \mathbb{R}^{n_x} \to \mathbb{R}^{n_x}$ is the nonlinear part of the vector field; and the state is $x = [x_s; \dot{x}_s; x_a]$. Note that, for the nonlinearities considered here (4.6), f^{NL} (and thus also $\nabla_x f^{NL}$) does not depend on the speed.

Following the notation in section 3.1, V_H will denote the speed at which the nominal system undergoes a Hopf bifurcation, and after which it will potentially exhibit limit cycle oscillations. Given a subcritical speed $\bar{V}_0$ (such that $\bar{V}_0 < V_H$ corresponds to a stable equilibrium) and the definition of a vector δ of parametric uncertainties, then the distance in the parameter space of the equilibrium at $\bar{V}_0$ from the closest Hopf bifurcation is computed by means of the robust bifurcation margin k_m. The robust bifurcation analysis will thus allow the quantification of the influence of parametric uncertainties on the onset of LCO, which are a notorious problem for nonlinear aeroelastic systems [11].

Numerical continuation can be applied to (4.7) after having specified the value of the trim state x_t. Two cases will be considered, case 1 ($c1$) with $x_t = 0$ and case

2 ($c2$) featuring a non-zero value $\alpha_t = 1^\circ$ for the angle of attack of the section. The latter is physically motivated by the fact that the section is generating positive lift to counterbalance gravitational forces directed downwards. Figure 7 shows the standard (i.e. nominal) bifurcation diagrams with V on the x-axis and the normalized plunge DOF $\frac{h}{b}$ on the y-axis (in the case of branches of LCO solution branches, this is the maximum value over a period). The usual convention of representing stable steady-states (equilibria and LCOs) with solid lines and unstable ones with dashed lines is adopted, and the Hopf bifurcation is marked with a circle.

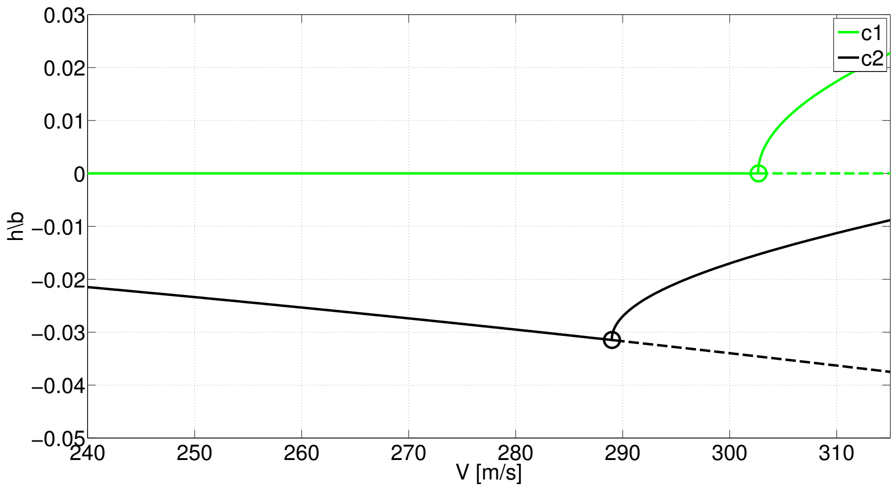

FIG. 7. *Bifurcation diagram for the nominal vector field for two different trim states.*

The system experiences supercritical Hopf bifurcations at V_H= 302.7 $\frac{m}{s}$ for $c1$ and V_H= 289.0 $\frac{m}{s}$ for $c2$. The frequency of the associated imaginary eigenvalues are respectively ω_H=70 $\frac{rad}{s}$ and ω_H=75 $\frac{rad}{s}$.

4.2.2. Computation of robust bifurcation margins. Including uncertainties in the nominal vector field of (4.7) yields the expression for the uncertain vector field

$$\dot{x} = \tilde{f}(x, V, \delta) = \tilde{\mathcal{A}}^L(V, \delta)x + \tilde{f}^{NL}(x, V, \delta), \tag{4.8a}$$

$$\tilde{J}(x, V, \delta) = \tilde{\mathcal{A}}^L(V, \delta) + \nabla_x \tilde{f}^{NL}(x, V, \delta). \tag{4.8b}$$

The bifurcation parameter V will be fixed in the subsequent analyses to $\bar{V}_0 = 270\frac{m}{s}$, which, recall Figure 7, is associated in both cases with stable equilibria –and hence, it is a valid choice according to the discussion in section 3.1.

The initial step to compute robust bifurcation margins is the definition of the nominal system and of the uncertainty set, which in turn will drive the construction of the underlying LFT. The former is described by (4.7), while the uncertainty definition is chosen to define a range of variation of $\pm 10\%$ from the nominal value for the coefficients $M_{s_{11}}$, $M_{s_{22}}$, $K_{s_{22}}$ and of $\pm 5\%$ for $M_{s_{12}}$ and $K_{s_{11}}$

$$\Delta_u = \mathrm{diag}(\delta_{K^L_{s_{22}}}, \delta_{K^L_{s_{11}}}, \delta_{M_{s_{11}}}, \delta_{M_{s_{12}}}, \delta_{M_{s_{22}}}). \tag{4.9}$$

This uncertainty definition was considered since it is the same as that used in [25], where the linear problem (i.e. $K_h^{NL} = K_\alpha^{NL}$=0) was extensively analyzed by means of nominal (eigenvalue analysis) and robust (μ analysis) techniques. This testcase is thus used to benchmark the first set of numerical results obtained with the method proposed in this paper.

Program 3.2 is computed with an initialization provided by the nominal values of the equilibrium point and of the uncertainties. The results from the program are reported in Table 5 in terms of robust stability margin k_m, frequency $\hat{\omega}$ of the imaginary eigenvalues at $\bar{V}_0$, and type of Hopf bifurcation. Recall indeed that Program 3.2 calculates the closest Hopf bifurcation without constraining the value of l_1, and the type of predicted Hopf bifurcation was assessed a posteriori with numerical continuation of the perturbed system.

TABLE 5
Robust bifurcation margins at $\bar{V}_0 = 270\frac{m}{s}$ for uncertainties in the set (4.9).

	k_m	$\hat{\omega}$ $\frac{rad}{s}$	type
c1	0.73	71.5	super
c2	0.49	75.1	super

It is inferred from the first column of Table 5 that in both cases the Hopf bifurcation could be shifted to $V = 270\frac{m}{s}$ within the uncertainty range (note indeed that $k_m < 1$). Another important observation is that $c1$ gives a margin k_m within less than 1% of the result from the literature [25] (obtained with μ considering the linear system at the same speed $V = 270\frac{m}{s}$). The (normalized) uncertainty vector found here by the optimizer is

$$\begin{aligned} \hat{\delta} =&[\delta_{K^L_{s_{22}}}; \delta_{K^L_{s_{11}}}; \delta_{M_{s_{11}}}; \delta_{M_{s_{12}}}; \delta_{M_{s_{22}}}], \\ =&[-0.7328; 0.7328; -0.7328; 0.5027; 0.7328], \end{aligned} \tag{4.10}$$

which also features the same perturbations (within a small tolerance) as those detected in [25] (their physical meaning in relation to the onset of flutter was discussed in the reference). In order to better appreciate the importance of this result, let us recall that nominal analyses (Figure 7) found for $c1$ the branch of equilibria at $x = 0$ regardless of V. Since the uncertainties selected here only affect $\tilde{\mathcal{A}}^L$, then $\tilde{f}^{NL}(0, V, \cdot) = f^{NL}(0, V) = 0$ and thus $\nabla_x \tilde{f}^{NL} \equiv 0$. That is, the determination of k_m is equivalent (for this specific case) to the problem solved by μ, i.e., finding the smallest perturbation matrix such that $\tilde{\mathcal{A}}^L$ is neutrally stable. The good matching with the literature results is very important, since in [25] μ_{LB} and μ_{UB} were shown to be close, indicating that the true value of μ was determined. This result hence verifies the correctness of the approach proposed here since it recovers the result which, for this specific case, is known a priori to be the correct one. Moreover, at least for this case, Program 3.2 is able to detect the global minimum of the optimization. Another positive feature is that Program 3.2 has the frequency ω as a decision variable, whereas μ was applied in [25] at discrete frequencies because this is the available implementation for the standard algorithms [2] (which has the drawback of possibly missing critical frequencies and thus overestimating the value of the stability margin).

Case $c2$ is then considered (with $\alpha_t = 1°$). This cannot be analyzed with μ because $\tilde{J}$ is now also a function of the nonlinear terms due to non zero values for the equilibria (which in turn depend on the uncertainty). For this reason, it is not possible to compare the results with the true analytic solution. However, it is noted that k_m now achieves a smaller value than for $c1$. This is in accordance with the nominal analyses in Figure 7, for which $c2$ presented a smaller V_H than $c1$. Thus, as $\bar{V} = 270\frac{m}{s}$ is closer to the nominal bifurcation speed for $c2$, a smaller robustness margin is expected. Note also that the two predicted frequencies $\hat{\omega}$ are relatively close to the nominal ones. These interpretations thus give some confidence that an accurate prediction of the margin has also been obtained for $c2$.

Other important information gathered in Table 5 is the type of closest Hopf bifurcations. Note that in order to obtain this result, the solver COCO was used to perform numerical continuation of the perturbed system, which also allowed verification that the latter experienced a Hopf bifurcation at $\bar{V}_0 = 270\frac{m}{s}$, as expected. These analyses show that the closest Hopf bifurcations are of the same nature as the corresponding ones in nominal conditions. Based on the greater attention typically devoted to subcritical LCOs due to the associated risks [11], the following analyses will make use of Program 3.4 to investigate whether changes in parameter values can drive the Hopf bifurcation from supercritical to subcritical. Without loss of generality, only the case $c2$ will be considered.

Uncertainties in two aerodynamic parameters are added to the set (4.9), namely, the terms $A_{0_{12}}$ and $A_{0_{22}}$ of the steady aerodynamics matrix A_0 (4.5). These correspond to the lift and moment coefficients of the airfoil respectively, and are allowed to vary within $\pm 20\%$ from their nominal values. Table 6 shows the solutions provided by Program 3.4 for the two types of possible Hopf bifurcation in terms of: Lyapunov coefficient l_1, stability margin k_m, frequency $\hat{\omega}$, and normalized perturbations. A tolerance $\epsilon_l = 1$ on the value of the Lyapunov coefficient was used.

TABLE 6
Worst-case perturbations and margins to supercritical and subcritical Hopf bifurcations.

	l_1	k_m	$\hat{\omega}\ \frac{rad}{s}$	$\delta_{K^L_{s_{22}}}$	$\delta_{K^L_{s_{11}}}$	$\delta_{M_{s_{11}}}$	$\delta_{M_{s_{12}}}$	$\delta_{M_{s_{22}}}$	$\delta_{A_{0_{22}}}$	$\delta_{A_{0_{12}}}$
super	-10^3	0.25	76	-0.25	0.25	-0.25	-0.25	0.25	0.25	-0.25
sub	1	3.13	67	-3.12	3.12	-3.12	-3.12	3.12	3.12	1.83

The supercritical case is consistent with the corresponding case in Table 5. Indeed, the margin approximatively halves as a result of the additional uncertainty in the system, while the frequency has a similar value. Note also that the constraint on l_1 is not active and thus l_1 has a large absolute value. On the contrary, the subcritical case features a far higher margin (which, according to the definition of k_m given in subsection 3.1, points out that there is no perturbation inside the allowed set capable of prompting the investigated bifurcation) and achieves a value of l_1 equal to the tolerance ϵ_l. Another interesting fact is that while all the normalized perturbations feature the same sign as in the supercritical case, this does not hold for $A_{0_{12}}$ which has an opposite perturbation and, in absolute value, smaller than the others. This is an interesting aspect, because according to standard interpretations of unstable aeroelastic phenomena [4, 25], a negative perturbation for $A_{0_{12}}$ would be expected (as noted for the supercritical case). The justification for this could be sought in the physical mechanisms prompting subcritical LCO [11] and will be investigated in future studies. It is remarked here that the commented scenario is distinctive of this problem, where different (possibly conflicting) constraints define the worst-case conditions. While robustness in the linear context focuses on the loss of stability only, from a dynamical systems perspective this becomes a multi-faceted concept characterized by concurrent conditions and thus non-intuitive results can be found.

Figure 8 shows bifurcation diagrams relative to worst-case combinations of parameters found by Program 3.4 by changing the tolerance on the Lyapunov coefficient

ϵ_l. In the legend of Figure 8, the value of the Lyapunov coefficient at the bifurcation point is indicated.

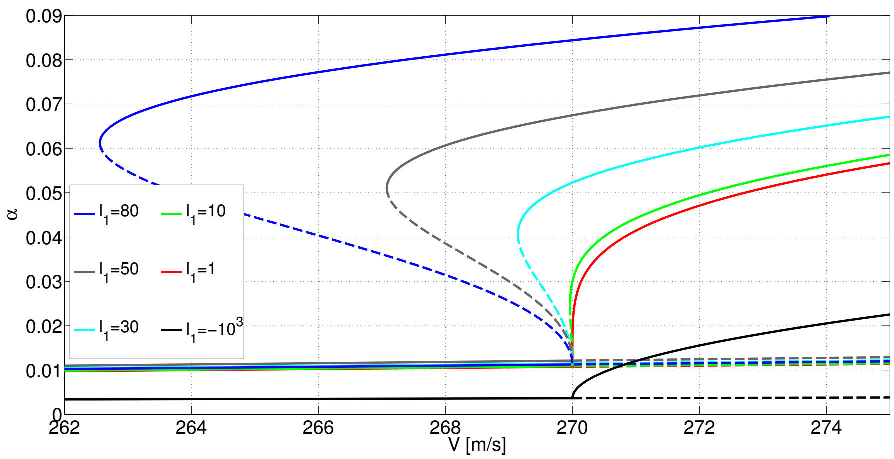

Fig. 8. *Bifurcation diagram of the system for different worst-case perturbations.*

The first important observation is that all the cases display a Hopf bifurcation at $\bar{V}_0 = 270\frac{m}{s}$. The branches relative to the solutions from Table 6 (obtained with $\epsilon_l = 1$) are $l_1 = -10^3$ and $l_1 = 1$. This in turn demonstrates that Program 3.4 is able to correctly predict worst-case combinations of uncertainty which lead to respectively supercritical and subcritical bifurcation. For the other curves $l_1 = \epsilon_l$ holds since this constraint is always active, and the associated margins k_m slightly increase compared to the value 3.13 featured in Table 6. It is stressed that a quantitative interpretation of the absolute value of l_1 depends on the arbitrary normalization adopted for the eigenvector q in its definition (3.10). The point made here is qualitative and, specifically, is that as the tolerance ϵ_l (and thus l_1) is increased, the subcritical Hopf bifurcation predicted by the optimizer is more pronounced (i.e. the range of speeds for which unstable and stable LCOs coexist with the branch of stable equilibria is larger). Even though this is not guaranteed by the Hopf bifurcation theorem, since l_1 is defined on the center manifold at the bifurcation point only, the magnitude of the Lyapunov coefficient can be taken as a measure of the subcriticality of the LCO (when comparing different instances computed with the same normalization of q). Figure 8 shows therefore that embedding the constraint on the Lyapunov coefficient in the bifurcation margin computation is successfully done by the optimization.

The last part of the section is aimed at providing insights into the numerical aspects of the algorithms. As a preamble, it is observed that there are not definitive answers with respect to robustness to local minima or efficiency of the algorithms as these will depend on many aspects such as, for example, the type of vector field (not only size and degree, but also number of attractors) and the optimization algorithm employed (which is an aspect that has not been investigated in this work). Investigation of these important features are left for future work.

The execution time of Program 3.4 is larger than that of Program 3.2 (approximatively $6s$ against $3s$ for the case with 7 uncertainties). Most importantly, the addition of the constraint on l_1 exacerbates the issue of local minima, especially when this is an active constraint. The set of strategies described in Section 3.3 were thus employed to obtain the results presented in Figure 8. Specifically, reinitializing the optimization with points on the auxiliary manifold $\mathcal{H}_g$ and with solutions obtained by fixing the frequency in Program 3.4 led to significant improvements in the solution.

Finally, it is remarked that for all the analyzed cases, the worst-case combinations of the uncertain parameters predicted by the optimization problem were used to perform numerical continuation analyses of the perturbed system with COCO. In all cases the perturbed systems encountered a Hopf bifurcation at the pre-selected speed $\bar{V}_0$. Even though this fact does not ensure that the global optimum (i.e. smallest margin to bifurcation) was found, it represents important evidence of the validity of the overall approach.

5. Conclusions. The paper develops a framework for the analysis of nonlinear systems subject to parametric uncertainties with the goal of studying robustness of stable equilibria to the onset of dynamic bifurcations. A scalar metric quantifying a perturbation in the uncertainty set is first defined, and the magnitude of the smallest perturbation such that a stable equilibrium is driven into a Hopf bifurcation point is named the robust bifurcation margin k_m. Its definition, which also allows the nature of the closest Hopf bifurcation (subcritical or supercritical) to be specified, is based on the idea of building a Linear Fractional Transformation model of the uncertain Jacobian and studying its singularity. The proposed margin can be interpreted as an extension of the structured singular value μ to the nonlinear context. The computation of k_m is recast as a nonlinear smooth constrained optimization problem, and as such it suffers in principle from the issue of local minima. Thus, the proposed programs technically provide only an upper bound on the margin. However, several mitigation strategies are described in order to tighten the gap with the actual margin, including a continuation-based multi-start strategy. Application of the framework is demonstrated on two case studies: a power system model and an aeroelastic system exhibiting nonlinear flutter behaviour. For the former, analyses show that k_m can be used to infer sensitivity of the Hopf bifurcation to system's parameters and it allows more accurate predictions than those achieved with available methods only providing first-order information. As for the latter, first the same results obtained in the literature with μ are retrieved, and then the possibility to distinguish between closest subcritical and supercritical bifurcations is explored. The results verify from different perspectives soundness of the newly introduced concept and provide examples of its perspective advantages over available techniques to study the nonlinear robustness problem in different application domains.

REFERENCES

[1] G. B. Arfken and H. J. Weber, *Mathematical methods for physicists*, Academic Press; 4th ed., San Diego, CA, 1995.

[2] G. Balas, R. Chiang, A. Packard, and M. Safonov, *Robust Control Toolbox*, 2009.

[3] W. Beyn, A. Champneys, E. Doedel, W. Govaerts, Y. A. Kuznetsov, and B. Sandstede, *Numerical continuation, and computation of normal forms.*, in Handbook of Dynamical Systems, Vol 2 / B. Fiedler (edit.), Elsevier, 2002, Chapter 4. - ISBN 0-444-50168-1, 2002, pp. 149–219.

[4] R. L. Bisplinghoff and H. Ashley, *Principles of Aeroelasticity*, Wiley, 1962.

[5] R. Braatz, P. Young, J. Doyle, and M. Morari, *Computational-complexity of μ-calculation*, IEEE Transactions on Automatic Control, 39 (1994), pp. 1000–1002.

[6] C. A. Canizares, *Calculating optimal system parameters to maximize the distance to saddle-node bifurcations*, IEEE Transactions on Circuits and Systems, 45 (1998), pp. 225–237.

[7] J. H. Chow and A. Gebreselassie, *Dynamic voltage stability analysis of a single machine constant power load system*, in 29th IEEE Conference on Decision and Control, 1990.

[8] G. Cirillo, G. Habib, G. Kerschen, and R. Sepulchre, *Analysis and design of nonlinear*

resonances via singularity theory, Journal of Sound and Vibration, 392 (2017), pp. 295–306.

[9] H. Dankowicz and F. Schilder, *An extended continuation problem for bifurcation analysis in the presence of constraints*, ASME 2009 International Design Engineering Technical Conferences and Computers and Information in Engineering Conference, 2009.

[10] H. Dankowicz and F. Schilder, *Recipes for Continuation*, Society for Industrial and Applied Mathematics, Philadelphia, PA, 2013.

[11] G. Dimitriadis, *Introduction to Nonlinear Aeroelasticity*, Aerospace Series, Wiley, 2017.

[12] I. Dobson, *Computing a closest bifurcation instability in multidimensional parameter space*, Journal of Nonlinear Science, 3 (1993), pp. 307–327.

[13] I. Dobson, F. Alvarado, and C. L. DeMarco, *Sensitivity of hopf bifurcations to power system parameters*, in [1992] Proceedings of the 31st IEEE Conference on Decision and Control, 1992.

[14] E. J. Doedel, T. F. Fairgrieve, B. Sandstede, A. R. Champneys, Y. A. Kuznetsov, and X. Wang, *Auto-07p: Continuation and bifurcation software for ordinary differential equations*, tech. report, 2007.

[15] J. Doyle, *Analysis of feedback systems with structured uncertainties*, IEE Proceedings D Control Theory and Applications, 129 (1982), pp. 242–250.

[16] J. Gerhard, W. Marquardt, and M. Monnigmann, *Normal vectors on critical manifolds for robust design of transient processes in the presence of fast disturbances*, SIAM Journal on Applied Dynamical Systems, 7 (2008), pp. 461–490.

[17] P. Gill, W. Murray, and M. Wright, *Practical optimization*, Academic Press, 1981.

[18] M. Golubitsky and D. Schaeffer, *Singularities and Groups in Bifurcation Theory*, Applied Mathematical Sciences, Springer-Verlag New York, 1985.

[19] W. Govaerts, *Numerical Methods for Bifurcations of Dynamical Equilibria*, Society for Industrial and Applied Mathematics, 2000.

[20] R. Gray, A. Franci, V. Srivastava, and N. E. Leonard, *Multiagent decision-making dynamics inspired by honeybees*, IEEE Transactions on Control of Network Systems, 5 (2018), pp. 793–806.

[21] J. Guckenheimer and P. Holmes, *Nonlinear Oscillations, Dynamical Systems, and Bifurcations of Vector Fields*, Applied Mathematical Sciences, Springer New York, 2002.

[22] M. Hayes, D. Bates, and I. Postlethwaite, *New tools for computing tight bounds on the real structured singular value*, Journal of Guidance, Control, and Dynamics, 24 (2001), pp. 1204–1213.

[23] R. Horn and C. Johnson, *Matrix Analysis*, Cambridge University Press, 1990.

[24] A. Iannelli, M. Lowenberg, and A. Marcos, *An extension of the structured singular value to nonlinear systems with application to robust flutter analysis*, 5th CEAS Conference on Guidance, Navigation and Control (EuroGNC), 2019.

[25] A. Iannelli, A. Marcos, and M. Lowenberg, *Aeroelastic modeling and stability analysis: A robust approach to the flutter problem*, International Journal of Robust and Nonlinear Control, 28 (2018), pp. 342–364.

[26] A. Iannelli, A. Marcos, and M. Lowenberg, *Study of Flexible Aircraft Body Freedom Flutter with Robustness Tools*, J. of Guidance, Control and Dynamics, 41 (2018), pp. 1083–1094.

[27] Y. Kuznetsov, *Elements of Applied Bifurcation Theory*, Springer-Verlag New York, 2004.

[28] J. Magni, *Linear fractional representation toolbox modelling, order reduction, gain scheduling*, Technical Report TR 6/08162, DCSD, ONERA, Systems Control and Flight Dynamics Department, 2004.

[29] A. Marcos, D. Bates, and I. Postlethwaite, *Nonlinear symbolic LFT tools for modeling, analysis and design*, in Nonlinear Analysis and Synthesis Techniques in Aircraft Control, L. N. in Control and S.-V. Information Science, eds., 2007.

[30] A. Marcos, D. Bates, and I. Postlewhite, *Control oriented uncertainty modeling using μ sensitivities and skewed μ analysis tool*, in IEEE Conference on Decision and Control, 2005.

[31] MATLAB, *Optimization Toolbox User's Guide*, 2014.

[32] A. Mazzoleni and I. Dobson, *Closest bifurcation analysis and robust stability design of flexible satellites*, Journal of Guidance, Control, and Dynamics, 18 (1995), pp. 333–339.

[33] Z. Michalewicz and D. Fogel, *How ro Solve It: Modern Heuristics*, Springer-Verlag, 2nd ed., 2004.

[34] M. Monnigmann and W. Marquardt, *Steady-state process optimization with guaranteed robust stability and feasibility*, AIChE Journal, 49, pp. 3110–3126.

[35] A. Packard and J. Doyle, *The Complex Structured Singular Value*, Automatica, 29 (1993), pp. pp. 71–109.

[36] A. Packard, M. Fan, and J. Doyle, *A power method for the structured singular value*, Proc.

of the Conference on Decision and Control, December 1988.

[37] A. Roberts, *Computer algebra derives correct initial conditions for low-dimensional dynamical models*, Computer Physics Communications, 126 (2000), pp. 187 – 206.

[38] A. Roberts, *Normal form transforms separate slow and fast modes in stochastic dynamical systems*, Physica A: Statistical Mechanics and its Applications, 387 (2008), pp. 12 – 38.

[39] C. Roos, *Systems modeling, analysis and control (SMAC) toolbox: An insight into the robustness analysis library*, in 2013 IEEE Conference on Computer Aided Control System Design (CACSD), 2013.

[40] C. Roos and J. Biannic, *A detailed comparative analysis of all practical algorithms to compute lower bounds on the structured singular value*, Control Engineering Practice, 44 (2015), pp. 219–230.

[41] W. D. Rosehart and C. A. Canizares, *Bifurcation analysis of various power system models*, International Journal of Electrical Power & Energy Systems, 21 (1999), pp. 171 – 182.

[42] M. Safonov, *Origins of robust control: Early history and future speculations*, 7th IFAC Symposium on Robust Control Design, June 2012.

[43] M. Safonov and M. Athans, *A multiloop generalization of the circle criterion for stability margin analysis*, IEEE Transactions on Automatic Control, 26 (1981), pp. 415–422.

[44] P. Seiler, A. Packard, and G. J. Balas, *A gain-based lower bound algorithm for real and mixed μ problems*, Automatica, 46 (2010), pp. 493–500.

[45] A. Taylor and W. Mann, *Advanced Calculus*, Wiley, 1983.

[46] V. Venkatasubramanian, H. Schattler, and J. Zaborszky, *Voltage dynamics: study of a generator with voltage control, transmission, and matched MW load*, IEEE Transactions on Automatic Control, 37 (1992), pp. 1717–1733.

[47] A. Yazici, A. Karamancioğlu, and R. Kasimbeyli, *A nonlinear programming technique to compute a tight lower bound for the real structured singular value*, Optimization and Engineering, 12 (2011), pp. 445–458.

[48] K. Zhou, J. C. Doyle, and K. Glover, *Robust and Optimal Control*, Prentice-Hall, 1996.